UNIVERSITY OF CALIFORNIA SAN DIEGO

Solid-Phase Processing Techniques of Optoelectronic Materials for Photovoltaic Applications

A dissertation submitted in partial satisfaction of the
requirements for the degree Doctor of Philosophy

in

Materials Science and Engineering

by

Guillermo Lazaro Esparza

Committee in charge:

Professor Darren Lipomi, Chair
Professor Carlos Coimbra
Professor David Fenning
Professor Ping Liu
Professor Nathan Romero

2023

The Dissertation of Guillermo Lazaro Esparza is approved, and it is acceptable in quality and form for publication on microfilm and electronically.

University of California San Diego

2023

DEDICATION

To those that fall down and get back up.

EPIGRAPH

I'm willing and able
To lift my dreams up out of their cradle
Nurse and nurture my ideals 'til they're much more than a fable
I can be all I can be and do much more than I'm paid to
And I won't be a slave to what authorities say do
My desire is to live within a nation on fire
Where creative passions burn and raise the stakes ever higher

Saul Williams

TABLE OF CONTENTS

LIST OF FIGURES

LIST OF TABLES

LIST OF SUPPLEMENTAL VIDEOS

Esparza_SFT_drum_setup.mp4

Esparza_SFT_large_area.mp4

Esparza_SPD_optical_microscopy.mp4

Esparza_SPD_snapback_optical_microscopy.mp4

Esparza_SPD_water.mp4

ACKNOWLEDGEMENTS

I would like to acknowledge Professor Darren Lipomi for his guidance, support, and friendship these last four years. I am glad that when you offered me a position in your lab, I took the chance and joined, despite knowing almost nothing about polymers at the time. It was, without a doubt, one of the best professional decisions I have ever made.

I would also like to acknowledge Professor David Fenning. You have been a font of knowledge since I took my first class with you and I have always appreciated your feedback and insight on my work. I am looking forward to finding out what else we can accomplish together.

I would also like to acknowledge my friends, peers, and assistants among the "Lipomi Homies." It is hard to imagine a better research group in which to have carried out my PhD and many of you played invaluable roles in helping my research come to light.

I would also like to acknowledge Professor Prabhakar Bandaru for helping me join the PhD program in the first place. Despite our professional relationship not ending on great terms, you helped me take my next academic step and I am grateful to you for it.

Lastly, I would like to acknowledge my family and loved ones, chief among them being my partner, Taylor McAdam, my mother, Angelina Garcia-Gomez, and my father, Luis Martinez-Baez. There have been many times in my life where, left to my own devices, my life would have taken dramatically different turns for the worse. You have provided me with love and support when I have needed it the most, and for this, I will be forever grateful.

The Introduction, in part is currently being prepared for submission for publication of the material. Guillermo L. Esparza, Darren J. Lipomi. The dissertation author was the primary investigator and author of this material.

Chapter 1, in full, is a reprint of the material as it appears in ACS Materials Letters 2021. Guillermo L. Esparza, Darren J. Lipomi, ACS Press, 2021. The dissertation author was the primary investigator and author of this paper.

Chapter 2, in full, is a reprint of the material as it appears in Advanced Materials 2023. Guillermo L. Esparza, Moses Kodur, Alexander X. Chen, Benjamin Wang, Jordan A. Bunch,

Jaden Cramlet, Rory Runser, David P. Fenning, Darren J. Lipomi., Wiley Press, 2023. The dissertation author was the primary investigator and author of this paper.

Chapter 3, in part is currently being prepared for submission for publication of the material. Guillermo L. Esparza, Deniz Cakan, Jaden Cramlet, Benjamin Wang, Jack Palmer, David P. Fenning, Darren J. Lipomi. The dissertation author was the primary investigator and author of this material.

VITA

2013	Bachelor of Science, Physics, Harvey Mudd College
2019	Master of Science, Materials Science and Engineering, University of California San Diego
2018-2023	Research Assistant, University of California San Diego
2023	Doctor of Philosophy, Materials Science and Engineering, University of California San Diego

PUBLICATIONS

Esparza, Guillermo L., and Darren J. Lipomi. "Solid-Phase Deposition: Conformal Coverage of Micron-Scale Relief Structures with Stretchable Semiconducting Polymers." ACS Materials Letters 3, no. 7 (2021): 988-995.
Esparza, Guillermo L., Moses Kodur, Alexander X. Chen, Benjamin Wang, Jordan A. Bunch, Jaden Cramlet, Rory Runser, David P. Fenning, and Darren J. Lipomi. "Solvent-Free Transfer of Freestanding Large-Area Conjugated Polymer Films for Optoelectronic Applications." Advanced Materials 35, no. 12 (2023): 2207798.

FIELDS OF STUDY

Major Field: Materials Science and Engineering

Studies in Optoelectronic Materials and Photovoltaics
Professors Darren Lipomi and David Fenning

ABSTRACT OF THE DISSERTATION

Solid-Phase Processing Techniques of Optoelectronic Materials for Photovoltaic Applications

by

Guillermo Lazaro Esparza

Doctor of Philosophy in Materials Science and Engineering

University of California San Diego, 2023

Professor Darren Lipomi, Chair

Optoelectronic materials and devices are ubiquitous in the modern world. Thin-film processing of these materials is essential in a tremendous range of applications such as consumer electronics, healthcare, defense, scientific instrumentation, and of particular relevance to this work, renewable power generation through photovoltaics. Typical processing of these materials occurs from either the vapor, liquid, or solution phases, but all of techniques come with various downsides and limitations. Much less common is the processing of thin films directly from the solid phase. That is, the creation of standalone thin films which are subsequently transferred onto the substrate. Such an approach is largely unexplored, and this work has focused on demonstrating some of the unique processing routes which become available when processing

from this phase. Particularly, this work focuses on: 1) The solid-phase processing of thin films of conjugated polymers to form conformal, functional coatings on textured light trapping surfaces. 2) The formation of freestanding films of conjugated polymers to then be transferred onto sensitive substrates (e.g. perovskites) to serve as a functional device layer, but applied in a manner that is devoid of liquid solvents. 3) The use of freestanding films of conjugated polymers as a sacrificial substrate onto which transparent conductive oxides can be sputtered, forming a freestanding bilayer, and subsequently transferred to complete perovskite solar cells without subjecting the sensitive perovskite layer to damage from the sputter process.

Introduction

Optoelectronic materials and devices are ubiquitous in the modern world. They are essential components in consumer electronics, healthcare, defense, scientific instrumentation, and more. Materials which interact both with light and electronic circuitry find application in almost every aspect of our lives. Of particular interest to the author is the application of these materials towards renewable power generation, especially solar cells, i.e. photovoltaics.

In order to form a functioning device, these materials are typically built-up in sequentially deposited layers, making the deposition of distinct materials an absolutely fundamental part of device fabrication. Typically, desired materials are deposited from either the vapor, liquid, or solution phases and condensed or frozen into the solid phase. Consequently, realizing a particular device architecture often requires that great consideration be placed in determining the compatibility of processing steps with the layers that have already been deposited. For example, deposition of a material might require high temperature or harsh solvents which might damage underlying layers, or a deposited material might be hydrophobic in a way that makes the subsequent step incompatible with processing from a solution. These are just a few of the many possible roadblocks that may be encountered in attempting to design a process flow for a desired device. Often, realizing a particular device architecture may be impossible with the available processes due to some sort of processing incompatibility. Thin-film processing from the solid-phase affords many new opportunities in processing. Not only can it address some limitations present when processing from other phases, but it can even enable entirely new processing routes that are highly distinct from anything previously possible.

There are many different types of optoelectronic materials. However, of particular

relevance to this dissertation is the processing of conjugated polymers and transparent conductive oxides. Conjugated polymers are distinguished by the hybridization of the p-orbitals along the polymer backbone. This hybridization causes the orbitals to extend along large segments of the chain, leading to a so-called delocalized orbital. These delocalized orbitals allow for intra-chain charge transport to occur along the backbone, as well π-π stacking interaction which allow for inter-chain charge transport.

Processing of these polymers is typically done from the solution phase where solid polymer has been dissolved in some solvent, and then this solvent is dispersed by a variety of different methods such as spin coating, slot die coating, and spray coating, among others[1]. Processing from the vapor-phase, where polymerization occurs in-situ, is possible[2]. However, this approach imposes significant restrictions on the molecular diversity that can be deposited. Many conjugated polymers require synthetic routes which make use of heterogeneous catalysis, or have monomers which are of too high a molecular weight, and therefore too low of a vapor pressure for deposition[3]. However, one advantage that vapor-phase deposition has over solution-phase processing is that it allows for deposition to occur conformally on a wide variety of different topographies. Such topographies are not possible to coat conformally using solution phase methods due to the influence of surface tension, which results in pooling and other non-uniformities to occur in the deposited film.

In the case of transparent conductive oxides (TCOs), these materials are almost always processed from the vapor phase. These materials are somewhat stoichiometrically complex and this makes their deposition challenging via some vapor phase processing routes, particularly evaporative methods[4]. This is because different species in the material will tend to have different vapor pressures. So, when evaporated, the resulting film will have a stoichiometry which is different from the source. In fact, the most typical technique to deposit transparent conductive oxides is by way of magnetron sputtering. In magnetron sputtering, a process gas, such as Argon, is used to strike a plasma where the plasma ions are made to impact a puck of material to be deposited, called a target. As the ions are driven by a DC or RF field, they impact the sputter

target and material is ejected from the target and condenses onto the surface of the desired substrate[5]. While the sputter yield does vary for different species, the stoichiometry of sputtered films tends to be much closer to that of the source material than evaporative techniques. However, unlike evaporative techniques, where the kinetic energy of the deposited atoms is often 1 eV, the kinetic energy of sputtered atoms can be in the 100s of eV[4]. This high energy, as well as reactive species from the process gas and target, results in an aggressive process that leads to various forms of sputter damage on the substrate.

As it pertains to photovoltaics, there are several processing challenges that we have sought to address by way of solid-phase processing. Light management is of critical importance in enhancing the efficiency solar cells. In silicon solar cells, this strategy is typically achieved by way of creating a highly textured, pyramidal surface on one or both faces of the silicon solar cell[6]. These pyramids are excellent light-trapping structures as they result in multiple incidence events for incoming light and also result in propagation of light along the plane of the cell (rather than straight through it), increasing the optical path-length. However, this texturing poses processing challenges using conventional methods when depositing additional materials, such as those for forming a perovskite solar cell, one of the most popular top-cell options explored today[7]. These issues arise particularly if the subsequent material to be deposited cannot be processed from the vapor phase. Examples of such materials would include the vast majority of conjugated polymers, which are commonly used as charge extraction layers in perovskite solar cells. Perovskite materials themselves are notorious for their sensitivity to stressors, and sensitive materials abound in many other fields. Such sensitivity can be particularly relevant when trying to process from solution, as various materials of optoelectronic relevance are only soluble in harsh solvents which may react in unfavorable ways with other layers[8]. Lastly, optoelectronic devices often require a conductive but transparent electrode, such as a TCO, the deposition of which is typically done via magnetron sputtering. Unfortunately, as discussed above, sputtering is an aggressive process that typically damages the underlying substrate. This damage is, again, particularly detrimental to sensitive materials such as perovskites, and normally requires a dense,

difficult-to-deposit buffer layer in order to protect the sensitive layer from significant damage[4]. All of these processing challenges are of significant research interest, and solid-phase processing provides potential avenues to address each of them.

It is the belief of the author that solid-phase processing can afford many new advantages and opportunities to the thin-film processing of various optoelectronic materials. All of the techniques discussed in this dissertation begin with the formation of a thin polymer film atop the surface of water via a process known as interfacial spreading[9]. In interfacial spreading a droplet of polymer solution is dropped upon the surface of water. With proper solvent selection, spreading of the polymer solution is driven by a reduction in interfacial free energy of the system. Once the polymer solution has spread the solvent quickly evaporates, leaving behind a thin polymer film atop the surface of the water. The thickness of this film can be tuned by a variety of parameters (solution concentration, droplet volume, and container size) and can range from tens to hundreds of nanometers (ca. 15-250 nm, in our studies).

Once a free-floating polymer film has been formed, it can be manipulated or otherwise made to behave in a variety of ways. In Chapter 1, we show how it can be used to form highly conformal, uniform thin-film coatings on micron-scale pyramids like those which would be found on the surface of a silicon cell. We do this with a variety of different conjugated polymers which are of interest as charge selective layers and generally cannot be deposited by vapor-phase processing. In Chapter 2, we show how processing from the solid phase allows one to manipulate pre-formed thin films by shearing them off the water surface, resulting in freestanding thin-films with exceptionally high aspect ratios (20 nm thick, 10×10 cm^2.) Once freestanding, the film can be dried and then transferred onto a substrate in a way that avoids exposure of the substrate to liquids solvents, as would typically occur when processing conjugated polymer from the solution-phase. Lastly, in Chapter 3, we show how these freestanding thin films of polymer can be used as an ultra-thin substrate onto which TCOs can be deposited via magnetron sputtering, resulting in a freestanding polymer/TCO bilayer film. In this method, the polymer film serves as a sacrificial layer, such that the sputtering process does not damage additional underlying layers.

This bilayer can then be manipulated or modified, such as by stripping the polymer (leaving behind a freestanding TCO-only film), and generally transferred onto a desired substrate in similar fashion to the freestanding conjugated polymer films of Chapter 2, though with additional challenges.

As many new and exciting materials grow in popularity, processing from the solid-phase is likely to enable unusual and unique processing routes that allow for previously difficult or impossible device architectures. Ultimately, the author believes that the area of thin-film solid-phase processing of optoelectronic materials is ripe for exploration and opportunity which requires much more exploration than one dissertation can realistically provide.

The Introduction, in part is currently being prepared for submission for publication of the material. Guillermo L. Esparza, Darren J. Lipomi. The dissertation author was the primary investigator and author of this material.

Chapter 1

Solid-Phase Deposition: Conformal Coverage of Micron-Scale Relief Structures with Stretchable Semiconducting Polymers

The manufacturing of semiconductor devices is enabled to a large extent by techniques that produce uniform thin films of polymeric materials. For example, spin-coating, slot-die coating, and various forms of chemical vapor deposition (CVD). However, just a small subset of these methods can coat substrates bearing topographic (relief) structures in a conformal manner. Meaning, few methods can form coatings in such a way that the thin film is uniform in thickness and the surface features are preserved with a high degree of fidelity. Moreover, methods that have this capability — e.g., polymer CVD — are limited to materials that can be polymerized in situ, and thus the diversity in the molecular structure of the deposited film is limited[2,10]. That is, there are currently no methods available to form conformal coatings of materials such as low-bandgap semiconducting polymers. Development of such a process would be useful, for example, in the field of photovoltaics, where silicon, perovskite, and organic semiconductors are commonly structured with relief as a means of trapping light[7,11–13]. Here, we describe a process inspired by water-based transfer printing, whereby a solid polymer film initially supported atop the surface of water can then be taken up by a topographically patterned substrate. This process — solid-phase deposition (SPD) — relies on plastic deformation of the polymer film to adhere to the relief structures in a conformal, defect-free way. It is applicable to a wide variety of polymers

of varying complexity and function to form conformal coatings of nanomenter-scale thicknesses on surfaces with micro-scale relief features. In this work, we used silicon textured with random pyramids with heights on the order of 10 μm. Such substrates were chosen both to demonstrate the capability of SPD to coat features which are much larger than the coatings are thick, as well as because prior work has shown that the reflectance of textured silicon surfaces significantly increases if the pyramids are too small (less than approximately 2 μm).[6]

Thin polymeric films are ubiquitous in science and technology. Along with photoresists—which have enabled essentially all of modern electronics—familiar examples in consumer electronics are anti-reflective[14] and anti-smudge coatings[15]. In biotechnology, polymeric films are used as mimics of cell surfaces[16], and chemical patterning of surfaces is ubiquitous in commercial genomics[17]. In the next generation of thin-film photovoltaics, polymeric thin films can serve as electron- and hole-transport layers. However, to maximize light absorption in thin-film solar cells[18], it may be necessary to use surface relief structures, as is common in silicon solar cells[19].

Conventional techniques such as spin-coating and spray-deposition can be used cover micron-scale topographic features. However, these techniques generally either have a planarizing effect for thick films, obscuring the surface features, or lack uniformity for thin films, as solution tends to pool in concave features and leave convex features bare. Polymeric coatings can be applied to relief structures with high uniformity using a number of techniques, which can be categorized as either "graft-to" or "graft-from" approaches[20]. In "graft-to" processes, pre-formed polymers can be covalently or electrostatically bound to surfaces which bear reactive groups (or intrinsic reactivity to end groups on the polymers[21]) or bound charges[22]. For example, fluorinated monolayers terminating in silane groups are used to coat touch screens[23]. Layer-by-layer assembly is a process by which polyanions and polycations are coated onto surfaces in an alternating manner[24]. Electrostatic forces ensure the formation of uniform layers.

In "graft-from" processes, the polymerization occurs directly on the surface[25]. Well known examples include various forms of controlled radical polymerization, notably atom-

transfer radical polymerization (ATRP)[26]. In surface-initiated ATRP, an alkyl bromide serves as the site of initiation of the chain-growth process. Surface-initiated ATRP proceeds in the solution phase. In contrast, polymers formed by polycondensation reactions can be formed on surface in a vapor-phase process known as molecular-layer deposition (MLD)[27]. In this process—applicable only to AB-type polymers—A and B monomers are alternately reacted with the surface in an iterative fashion. Lack of self-reactivity of like monomers ensures uniform thickness of a monodisperse coating. A solution-phase process which is otherwise analogous to MLD, termed molecular layer-by-layer deposition, has also been demonstrated.[28] Other than MLD, relevant vapor-phase processes fall under the general category of polymer CVD[2]. Like MLD, polymer CVD is applicable to a variety of substrates, including topographically complex surfaces such as textiles[29]. Significant advances have been made in reactive vapor deposition of relatively simple conjugated polymers such as polythiophenes and poly(phenylenevinylenes)[30]. However, polymer CVD is generally limited to reactive monomers and/or those with a low molecular weight.

While powerful, these techniques are not applicable to polymers which can only be polymerized using conventional, solution-phase chemistry. For example, polymers whose formation requires heating (and possibly reflux), heterogeneous catalysts, redox processes, and harsh solvents may not be amenable to coating by existing methods. These polymers include essentially all low-bandgap π-conjugated (semiconducting) polymers used in research in photovoltaics, thin-film transistors, light-emitting devices, and biosensors. New methods are thus needed for the deposition of pre-formed polymers on surfaces bearing micron-scale relief features.

Our laboratory has had a long interest in the mechanical properties of conjugated polymers, especially in ways to combine mechanical deformability with good charge-transport properties[31]. For example, we have previously demonstrated the ability to transfer films of stretchable bulk heterojunction films to hemispherical surfaces[32], though these surfaces did not impose the greatest possible mechanical demands on the films. We thus sought to develop a

method whereby physical transfer and subsequent deformation of a pre-solidified film could be used to obtain conformal coverage of topographic surfaces—even those bearing sharp features—with substantially more uniformity than it was previously possible to achieve. We were inspired by the work of Rogers et al. in the area of kinetically controlled transfer printing[33], and also by the common industrial process known as water transfer printing[34].

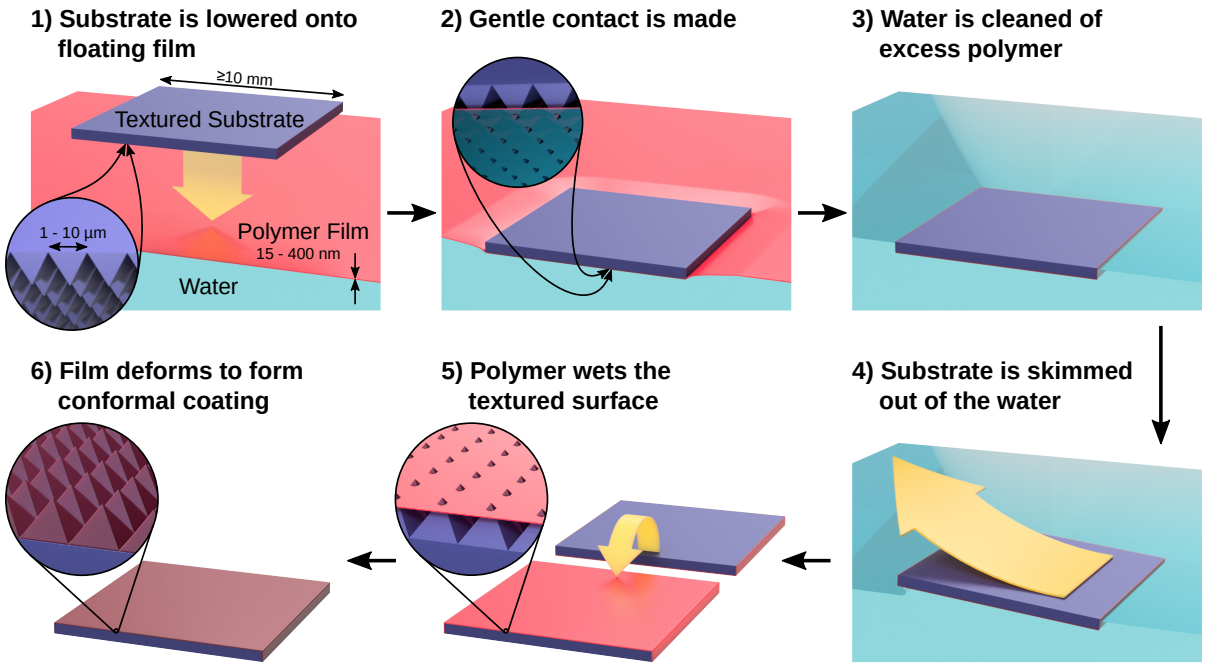

Figure 1.1. Summary of a solid-phase deposition process, taking place in ambient conditions. A polymer film suspended on water is taken up by a textured substrate with high-energy surfaces, enabling the necessary deformation of the polymer as it conformally coats the substrate.

The SPD process is shown schematically in Figure 1.1. Unless otherwise noted, this was the process used throughout this work. SPD begins by suspending a pre-solidified polymeric film on the surface of water, in a process known as solution spreading[9]. The process of transferring this film to a substrate is independent of the method used to produce the film, but we chose solution spreading for its simplicity. Solution spreading relies on the Gibbs-Marangoni effect to drive the spreading of a polymer solution atop the surface of water. Evaporation of the solvent results in the formation of a solidified polymer film, which remains suspended at the water-air interface. The process of transfer begins by pressing the substrate into the floating film with

the relief structures (pyramids) oriented downward (step 1). Upon contact with the polymeric film (step 2) and before lifting the substrate from the surface of the water, excess polymer was manually cleared from the perimeter of the substrate using a tool (step 3). The substrate (bearing the polymeric film underneath) is skimmed from the surface (step 4) and inverted (step 5). Given favorable ductility of the polymeric film and adhesion to the substrate, the conformal coverage takes place spontaneously (step 6). Various stages of the wetting process are shown in Figure 1.2; footage corresponding to Figure 1.2c can be found in the Supplemental Video: Esparza_SPD_optical_microscopy.mp4.

We found that the ability to obtain conformally coated films was a product of the surface energy of the substrate as well as the dimensions and mechanical properties of the polymeric films. In our experiments, we found it necessary to render the substrates hydrophilic using an air plasma. In contrast, treating the substrates with a hydrophobic silane monolayer led to poor transfer. The cause for this effect is two-fold: The hydrophilic surface promotes wetting by the polymer film itself, but it also allows for the intrusion of water into the polymer-substrate gap by capillary action. Entry of the water occurs from the edges when the excess polymer is removed (step 3 in Figure 1.1). In a way that will be described in more detail later, the presence of the water facilitates the conformal coating on a topographic substrate. Because the film is initially planar, the deformation it must undergo is significant. Thus, films with low stiffness, low yield strength, high ductility, low thickness, or a combination of these properties, produced conformal coatings with the fewest defects. Good results were obtained for many semiconducting polymer films under ambient conditions. Nevertheless, for films of polymers with greater stiffness, yield strength, brittleness, or thickness, it was possible to use solvent vapor, or other means, in order to induce plasticization and permit conformal coating. We will discuss these "assisted" methods of SPD later.

To investigate the roles played by the extensive and intensive properties of the polymeric films on the SPD process, we performed experiments using a variety of poly(3-alkylthiophenes) (P3ATs, Figure 1.3) as the model materials. In particular, we varied the length of the side chain

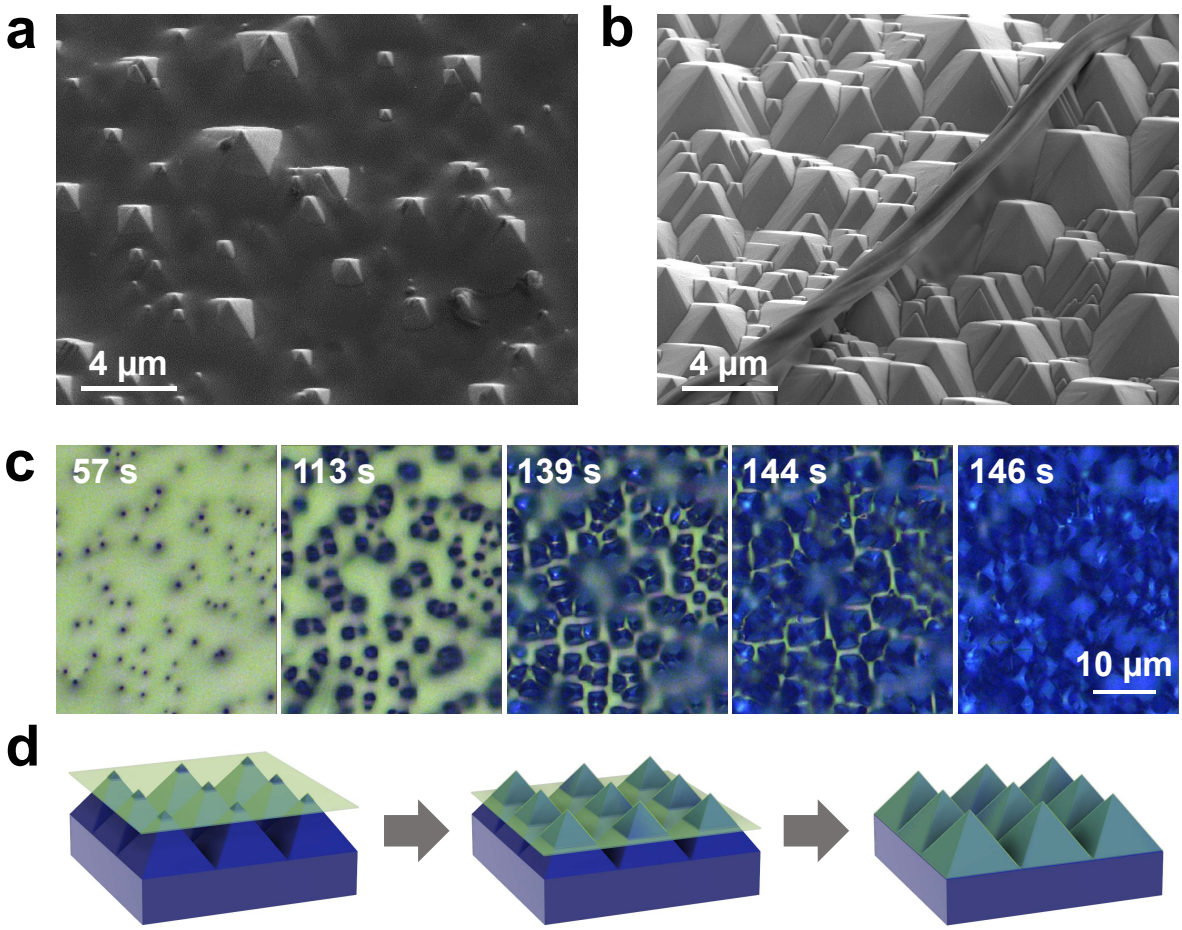

Figure 1.2. Evolution of the wetting process. a) A scanning electron micrograph (SEM) of a polymer film which partially coated the pyramidal peaks of a textured silicon substrate b) An SEM of another polymer film which has wetted a textured silicon substrate. The top left region shows bare pyramids, while the bottom-right region has been conformally coated, leading to the contrast between the two regions. The feature crossing the SEM diagonally is a rolled-up portion of the film, the continuation of which can be seen immediately below the roll as the film joins with the surface. c) Still frames with time-stamps from an optical microscopy video showing the same sample area as a polymer film progressively wets the surface of a pyramidal silicon substrate. d) Schematic illustration showing the progression of the wetting process after the film has been transferred.

(m) in order to tune the intrinsic deformability, while keeping the pre-transfer thickness (t_0) constant. We also varied t_0 while keeping m constant ($m = 7$). In these experiments, P3AT films were transferred onto comparable, plasma-treated substrates and SPD was allowed to proceed in ambient conditions until no further evolution of the coating process was observed. The endpoint of each experiment was measurement of the "equilibrium fractional conformal coverage," ϕ_f. We

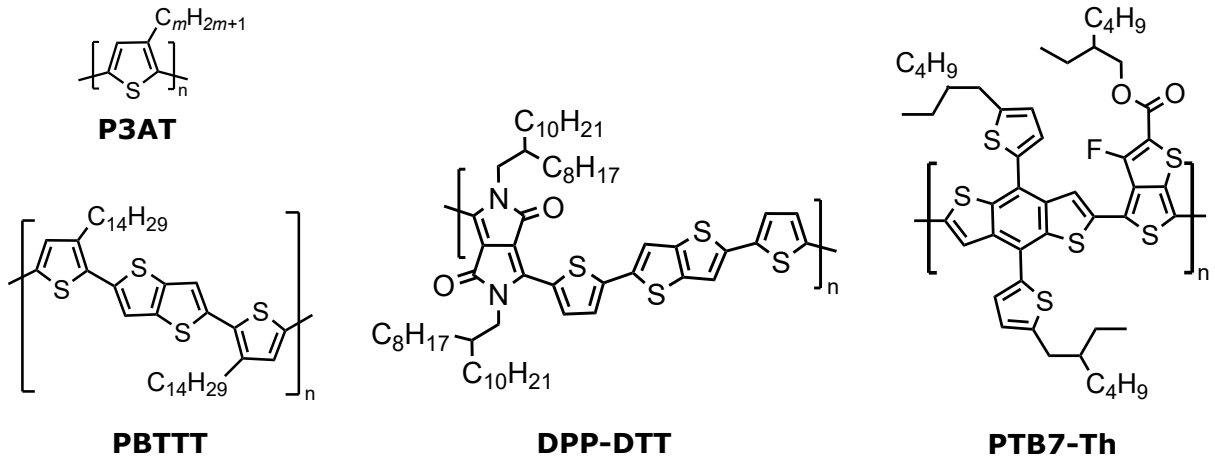

Figure 1.3. Chemical structures of the conjugated polymers discussed in the text

define the fractional conformal coating of the system as

$$\phi = \frac{A_{\text{conf}}}{A} \tag{1.1}$$

where A is the total pyramidal area in view, and A_{conf} is the pyramidal area which has been coated. Measurement of ϕ_{f} was done by collecting top-down scanning electron micrographs (SEMs) of the samples and using image analysis methods to segment the image, allowing for determination of A_{conf}. The results of these experiments and a sample of the SEM data used are shown in Figure 1.4a, b, respectively.

The cause for the incomplete conformal coverage ($\phi_{\text{f}} < 1$) in these experiments was the occurrence of a what we will refer to as "snap-back." Snap-back is characterized by the rapid recession of the film from the underlying substrate surface after wetting has already occurred, as depicted in Figure 1.4c. Once snap-back has happened in a given region, further wetting of the substrate surface was not observed. Snap-back was also observed to nucleate and then propagate throughout the rest of the sample. This nucleation is seen in the Supplemental Video: Esparza_SPD_snapback_optical_microscopy.mp4, along with additional optical microscopy footage of the snap-back behavior taking place.

The extent of snap-back is quantified by ϕ_{f}, and the observed dependencies of ϕ_{f} on m

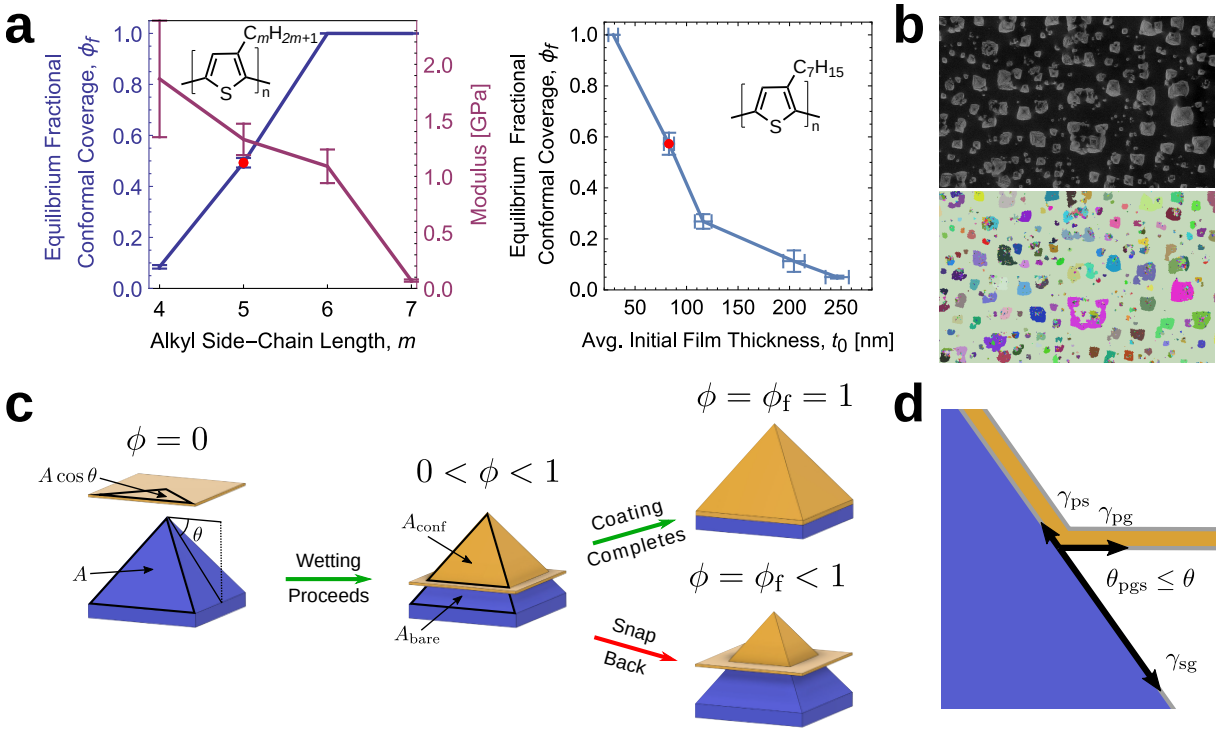

Figure 1.4. Fractional conformal coverage. a) SPD was performed using various P3AT films. (Left) ϕ_f was measured for films stamped with P3ATs of different side-chain lengths, m. Also shown are literature values of the moduli for the same P3ATs, as measured by the buckling technique[35]. (Right) ϕ_f was measured for P3HpT films of varying initial thickness, t_0. The red data points indicate conditions which led to some samples of a "mixed state," where snap-back occurred over part of the sample, but completed over the rest. Only regions of the of the former were used in calculating the point value. b) A sample of raw SEM data (top) and the same data after image segmentation (bottom), used to perform a measurement of ϕ_f. c) A schematic diagram of the possible evolutions of the wetting process. The films were either observed to complete coverage (top fork) or undergo "snap-back" and stop (bottom fork.) d) A cross-sectional diagram of the polymer-substrate-gas interface. The vectors show the relative magnitudes of the interfacial energies, as estimated from contact angle measurements. The represented system has P3HpT as the polymer, air-plasma treated/oxidized silicon as the substrate, and air as the gas. $\gamma_{sg} = 76.3$ mJ m^{-2}, $\gamma_{pg} = 28.6$ mJ m^{-2}, and $\gamma_{ps} = 11.5$ mJ m^{-2}.

and t_0 can be explained by considering how the total strain-energy of the polymer, U, is expected to vary across the samples. In general,

$$U = \int_{V_p} u dV, \tag{1.2}$$

where u is the strain energy density and V_p is the total polymer volume. Additionally, it is well

understood that all else being equal, the mechanical properties of P3ATs vary monotonically as a function of m. An increase in m results in a decrease of tensile modulus, yield strength, and ultimate tensile strength and an increase in fracture strain[31]. In short, P3ATs with a larger m are more compliant, will show a lower u for a given strain, and u will grow less rapidly as the strain occurs. Given that the films are much thinner than the pyramids are tall, it may be reasonable to assume that different films will display similar overall strain distributions for a given ϕ as the film makes its initial descent. If so, it follows that the strain energy required to trigger snap-back will be reached at lower values of ϕ for less compliant polymers due to a more rapid increase of u, or for thicker films due to a larger V_{p}. Based on this analysis, it is logical to put forward that SPD is facilitated when the polymer is above its glass transition temperature, as is the case for P3HpT and P3HT in ambient conditions. However, it should be emphasized that film thickness, as well as other factors such as the geometry (e.g., the complexity of the topography), are likely to influence the quality of the coated film.

It is evident that the mechanical properties of the polymer films play a significant role in facilitating (or frustrating) the SPD process, but the driving mechanism remains unexplained. Given that successful coatings have only been observed when the substrate is rendered hydrophilic, it may appear that SPD is driven by a reduction in interfacial free energy. Indeed, the interfacial tensions between the substrate, polymers, and air (as estimated by contact angle measurements) indicate that the advancement of the triple interface down the slope of the pyramid is energetically favorable. This scenario is depicted in Figure 1.4d, where the restricted geometry at the triple interface is expected to ensure an imbalance of interfacial tensions. However, dry films transferred directly onto the substrates (i.e., without being suspended on water), do not show significant wetting. This result indicates that the simple description above is incomplete, and implies that water is playing an active role in SPD.

As previously mentioned, SPD involves the presence of water between the polymer film and the substrate. The presence of water was verified by performing a series of coatings where, partway through the wetting process, a dry cleanroom swab was used to wipe away half of the

film. For every sample examined in this way, wiping away the film revealed a thin layer of water which visibly evaporated. The evaporation of water was shortly followed by completion of the coating on the other half of the substrate (where the film had not been wiped away), indicated by a visible change in color. Sample footage of this process can be found in the Supplemental Video: Esparza_SPD_water.mp4. We believe the film deformation involved in SPD is primarily driven by this water, which is adhered to both the polymer film and the substrate, and fills the void between them. As water molecules enter the gas phase after diffusing through the film, the volume of water is reduced. It is generally unfavorable to form a gas-liquid interface, and so the water continues to adhere to the film as its volume decreases, pulling the film down and deforming it. However, if the strain energy stored in the film is sufficiently high, then a gas-liquid interface will form, resulting in a "headspace" as the water and film de-adhere, which manifests as "snap-back." This final point is supported by the second clip in the Supplemental Video: Esparza_SPD_snapback_optical_microscopy.mp4, which clearly shows how the film dramatically changes color once a region has snapped back. The change in color indicates a change in the index of refraction of the medium backing the film, which goes from water to a gas.

For sufficiently compliant polymeric thin films, the SPD process can complete unassisted, with fractional conformal coverage approaching unity. However, to make the process amenable to stiffer films, we explored various methods of in situ plasticization. The aim of these methods is to soften the film so that the stored strain energy is dissipated quickly, thereby making snap-back or mechanical failure less likely. One of these methods is to transiently plasticize a transferred film by exposing it to the vapor of a low-boiling solvent (e.g., chloroform) in an enclosed chamber. This solvent-vapor assisted process proved effective in enabling conformal transfer of various polymeric films at a wide range of thicknesses. Figure 1.5 shows cross-sectional scanning electron micrographs taken of two comparable samples stamped with thick P3HpT films. For one sample, SPD was allowed to evolve in air and snap-back occurred. For the other, the sample was exposed to chloroform vapor immediately after film transfer. The vapor was supplied from a heated source (60 °C) and exposure was done for 10 min. The resultant coating is generally

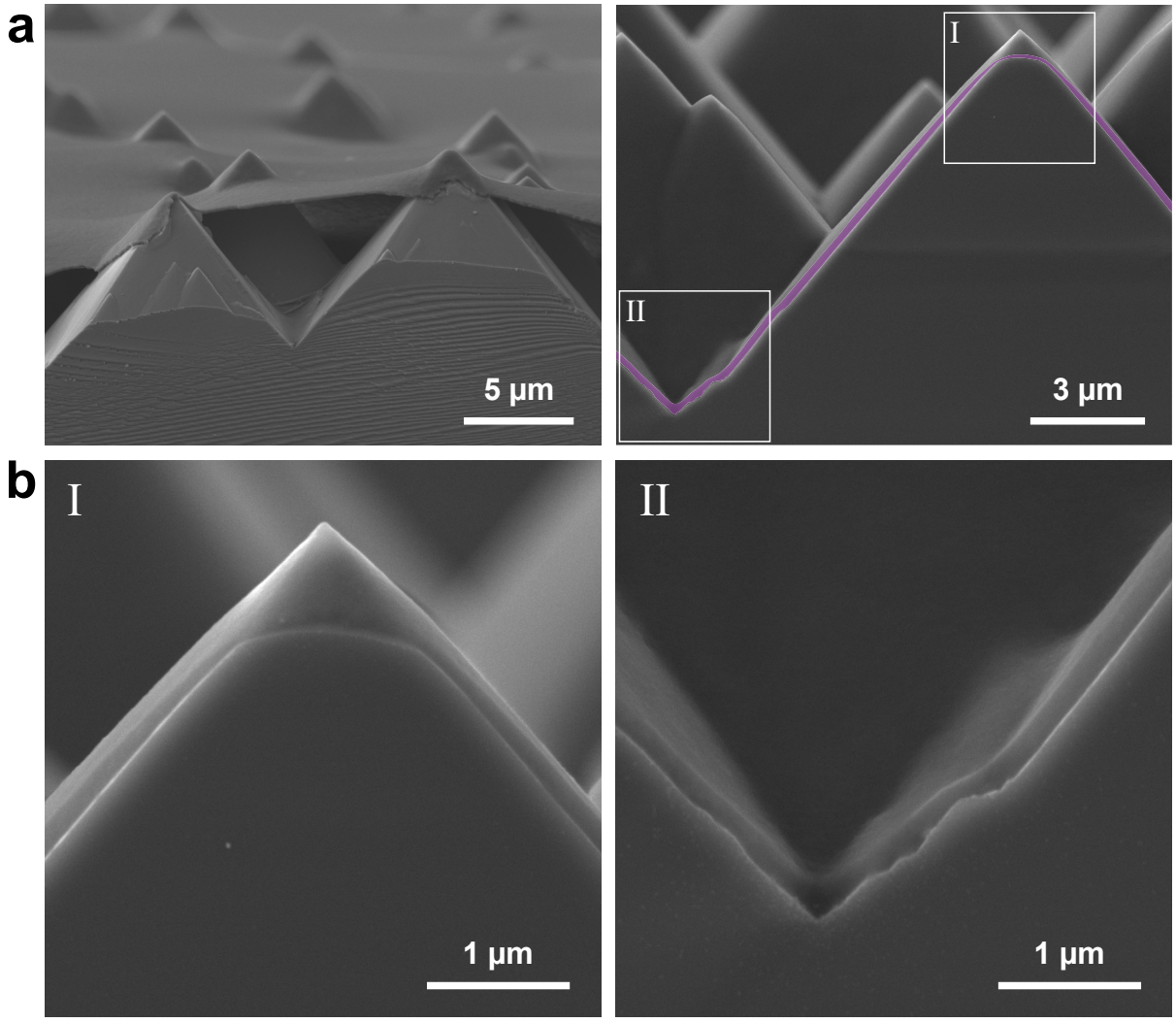

Figure 1.5. Results of the SPD process when assisted by solvent vapor. a) (Left) Cross-sectional SEM of a thick P3HpT film which underwent snap-back, and (right) an analogous sample which was exposed to chloroform vapor (60°C for 10 minutes). The polymer cross-section is shown in false color for clarity. b) Magnified regions of the right frame from section (a); the micrographs show how the film thins at the pyramid apex but otherwise remains uniform throughout.

uniform, though the film was consistently observed to thin near the apexes of the pyramids, presumably due to a concentration of force at those sites. It is possible that this thinning could be reduced or avoided by using pyramidal substrates with peaks of larger radii of curvature. Pyramids of decreased sharpness are already standard in the silicon photovoltaics industry, as overly sharp pyramids cause issues relating to dopant diffusion, among other problems. Additional micrographs showing the thinning at the apex can be found in Figure 1.7. For

comparison, cross-sectional micrographs of pyramidal substrates which were spin-coated with P3HpT using various conditions can be found in Figure 1.8. These samples display various defects, such as pooling between pyramids as well as uncoated peaks and sidewalls, which arise with such an approach.

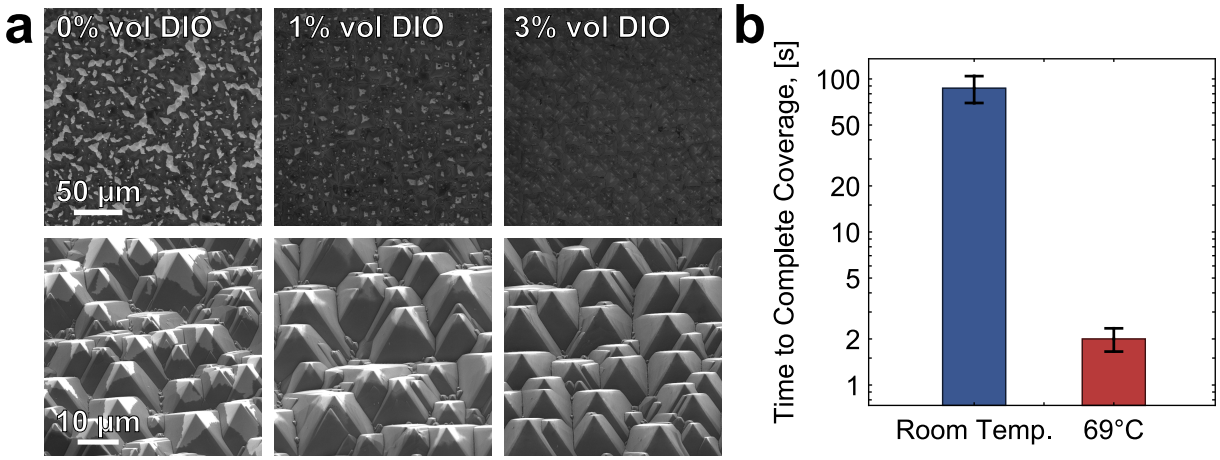

Figure 1.6. Use of cosolvent additives and increased temperature to increase the fractional coverage and speed of the coating process. a) (Top row) top-down micrographs of DPP-DTT coating bare pyramidal silicon, and exposed to chloroform vapor after transfer. From left to right, there was an increasing amount of DIO included in the polymer solution used to derive the film. Lighter regions show bare silicon. These micrographs were captured with an in-lens detector. (Bottom row) the same samples, at higher magnification and viewed from an angle. b) Chart showing the measured time from initial transfer to complete coverage for samples allowed to evolve at two different temperatures. The substrates were bare silicon, coated with a thin P3HpT film ($t_0 \approx 25$ nm), and allowed to evolve in air.

In addition to the use of solvent vapor as a means of temporary plasticization, it is possible to achieve a similar effect by including high-boiling cosolvents in the solutions from which the films are solidified. These minimally volatile additives function as traditional plasticizers, and some have the added benefit of improving the performance metrics of thin-film transistors and solar cells. This method was explored with the addition of 1,8-diiodooctane (DIO) to solutions of DPP-DTT, a low-bandgap polymer. DPP-DTT is a donor-acceptor polymer of technological interest due to its low bandgap, air-stability, and exceptionally high hole mobilities[36]. However, attempts to coat this polymer from a neat solution, whether in air or assisted by solvent vapor exposure, resulted in significant fracturing of the films. For the bare silicon substrates we tested,

these defects occurred at the apexes of the pyramids. Interestingly, when tested on ITO-coated pyramids, the films were observed to fracture at the valleys between pyramids. In both cases, the inclusion of small quantities of DIO ($\leq 3\%$ by premixed volume of solution) significantly reduced the occurrence of these defects. Figure 1.6a shows these results for DPP-DTT on bare silicon. It should be noted that DIO, while facilitating SPD, actually makes the films more prone to fracturing under rapid mechanical insults. To accommodate this fragility, the method of polymer transfer differed from the others in this work in that the substrate was dipped directly into the water and used to scoop the polymer up from below.

Lastly, SPD can also be assisted by heating. Heating can accelerate the coating process by increasing the rate at which water is expelled from the polymer-substrate gap and is also expected to soften otherwise stiff or brittle films. Figure 1.6b shows the results of an experiment where thin P3HpT films ($t_0 \approx 25$ nm) were transferred onto bare silicon substrates. Coating was allowed to evolve either at ambient conditions or on a heated surface (69 °C). The average time to coating completion was reduced by almost two orders of magnitude for the heated samples compared to those at room temperature, from 87 ± 17 s to 2.0 ± 0.3 s.

We have found these methods to assist SPD to be suitable in most scenarios, but some polymers remain too brittle for successful transfer (e.g., PBTTT, Figure 1.3). The side-chains of PBTTT are known to interdigitate, resulting in exceptionally high crystalline fractions[37]. This degree of crystallinity makes the PBTTT films exceptionally brittle and they have never survived the transfer process in our hands. The polymer still adheres to the pyramid walls, but fractures at the single micron scale, creating completely discontinuous coatings (Figure 1.9). All of the polymers which we have attempted to form SPD coatings with, along with the methods which have been successful, are detailed in Table 1.1.

Two possible use cases of SPD which are of particular interest to us include the application of charge-selective layers in silicon/perovskite tandem cells as well as enhanced light management in organic photovoltaic (OPV) devices. The majority of this work pertains to neat polymer films and is therefore most applicable to the former use case. On the other hand, use

Table 1.1. The polymers with which SPD has been attempted, the SPD method/s used which were successful ("SPD" corresponds to no assistance, "sv" to solvent vapor, "cs" to cosolvent, and "h" to heated), the type of pyramidal silicon substrate used (bare or ITO-coated), as well as previously published values for the modulus and crack onset strain (as measured by the so-called "buckling technique" and assimilated in[35])

Polymer	**Successful Method/s**	**Silicon Substrate**	**Modulus [GPa]**	**Crack Onset Strain [%]**
P3BT	sv	bare	1.87	6
P3PT	SPD, sv	bare	1.33	—
P3HT	SPD, sv	bare & ITO-coated	1.09	9
P3HpT	SPD, sv, h	bare	0.07	65
DPP-DTT	sv + cs	bare & ITO-coated	—	—
PTB7-Th	sv	bare	—	—
PBTTT	—	ITO-coated	0.879	$<$2.5

of SPD in OPV poses unique challenges. The efficiency and stability of OPV cells is highly dependent on the morphology of the bulk-heterojunction (BHJ) active layer, in which a polymeric donor and an acceptor are combined in an interpenetrating network. Moreover, BHJ films generally have poor mechanical properties, particularly when using fullerene acceptors. The poor mechanical properties would most likely require the use of one of the assisted methods to form high-quality coatings. However, these methods (meaning, the application of heat, solvent vapor, or cosolvents) are often what is used to arrive at a desired morphology. Therefore, employing SPD, particularly one of its assisted variations, could have a negative impact on the BHJ morphology. One possible approach to account for this issue could be to devise a means to slow SPD down such that the BHJ film can undergo very slow relaxation, thereby preventing snap-back while minimally disturbing the film morphology. However, the slowing of a manufacturing process is generally not desirable, and therefore the more likely approach to integrating SPD into the manufacturing of OPV cells would be to merge SPD with another step (such as thermal/solvent annealing) such that this single hybrid step produced a BHJ coating

that was both conformal and possessed the desired morphology. Micrographs of a BHJ film (P3HT:PCBM in 1:1 ratio) applied to ITO coated pyramids can be seen in Figure 1.10.

In summary, a novel process by which to apply uniform and conformal polymeric coatings to topographically complex surfaces has been introduced and explored. This process necessitates the formation of a pre-solidified film, here formed and suspended on the surface of water. The film is then mechanically taken up from the water surface by an activated substrate, and the process proceeds by leveraging or enhancing the plasticity of the film as the polymer wets the substrate surfaces. By appropriate tuning of the system parameters and materials selection, it is possible to form functional coatings in a range of thicknesses, in minutes or less, in or near ambient conditions. Moreover, the process is applicable to a wide range of polymers not otherwise possible to coat with using solution or vapor-phase processes. This process is not without its limits, as it appears to be incompatible with exceptionally brittle polymers and is unlikely to be applicable to substrates with reentrant surfaces (i.e., those with undercuts). It has also not been demonstrated over large areas, though solution spreading has been shown to be compatible with roll-to-roll processing,[38] and so the compatibility of SPD with textured, flexible substrates seems likely. Regardless, due to its simplicity, expediency, and flexibility, we believe SPD could impact a wide range of fields such as sensing, medicine, and energy. Our interests lie in how it may be used to enhance and enable novel photovoltaic devices. The past decade of work has signified both a resurgence in organic photovoltaics, as well as a massive surge in interest for hybrid organic/inorganic materials and devices. As the photovoltaics community continues to strive in enabling tandem cells for the next generation of utility-scale solar power production, we believe further developments in SPD may position it as a viable processing method in the manufacture of these devices.

1.1 Experimental Methods

1.1.1 General

All polymer solutions were made with chlorobenzene as the primary solvent, were magnetically stirred for >12 hours at approximately 60 °C, and were kept heated during experiments. Air plasma treatments were done using a RF plasma cleaner from Harrick Plasma. The plasma cleans were done at 30 W with a chamber pressure of approximately 300 mTorr. All solution spreading was done on deionized (DI) water in glass petri dishes with an inner diameter or 5.6 cm. A hydrophobic silane coating was applied to all petri dishes in order to increase the water contact angle and provide a more planar surface for spreading. This silane coating was applied by cleaning the dishes, followed by air plasma exposure to activate the glass surface, and completed by exposing the dishes to trichloro(1H,1H,2H,2H-perfluorooctyl)silane vapor under static vacuum. Pyramidal silicon substrates (bare) were prepared from fresh wafers by first cleaning the wafers in solvents (acetone, ethanol, isopropyl alcohol (IPA), and DI water, in that order). Cleaning was followed by stripping of the native oxide using dilute hydrofluoric acid. The pyramids were then etched into the wafers in heated (80 °C) potassium hydroxide solution with isopropyl alcohol as a surfactant, followed by rinsing in DI water.

1.1.2 Profilometry

The initial thickness of transferred films were estimated by using the same "spreading parameters" (drop volume, polymer solution concentration, and dish size) to form films which were transferred to planar (glass) substrates. Thickness of these films were then measured using a Dektak XT profilometer. For PTB7-Th, as the films were exceptionally thin (15 nm), 6 stamps were performed on the same substrate, from which the average thickness of an individual stamp was estimated.

1.1.3 Fractional Conformal Coverage Experiments

ϕ_f *vs* m: Solutions of P3BT, P3PT, P3HT, and P3HpT were prepared at 10, 10, 10, and 20 mg/mL concentrations (respectively) and filtered through polytetrafluoroethylene (PTFE) filters with a 0.45 μm pore size. Previously prepared pyramidal silicon substrates were cleaned in acetone, ethanol, IPA, and DI water, followed by 10 air plasma clean. Droplet volumes, tuned to produce films approximately of the target thickness (40 nm), were 10.28, 9.84, 6.14, 7.44 uL for P3BT, P3PT, P3HT, and P3HpT respectively. Three samples were prepared for every polymer material used. To account for any evolution of the plasma treated surfaces, the stamp order was randomized. Optical microscopy footage was captured for every sample, documenting the occurrence of snap-back. At least three top-down scanning electron micrographs were captured for every sample for later image analysis.

ϕ_f *vs* t_0: Solutions of P3HpT were prepared at 10, 20, 30, 40, and 50 mg/mL and filtered through PTFE filters with a 0.45 μm pore size. Previously prepared pyramidal silicon substrates were cleaned in acetone, ethanol, IPA, and DI water, followed by 10 min air plasma clean. 10 μL droplet volumes were used to form the films. Three samples were prepared for every concentration used. To account for any evolution of the plasma treated surfaces, the stamp order was randomized. Optical microscopy footage was captured for every sample, documenting the occurrence of snap-back. At least three top-down scanning electron micrographs were captured for every sample for later image analysis.

1.1.4 Image Analysis

The image analysis of micrographs was performed using an algorithm written in *Mathematica*, which made use of various built-in functions. Each image first binarized using `Binarize[]`. This was followed by application of `GradientFilter[]` to create outlines of the different regions. This then allowed for image segmentation using `WatershedComponents[]`. The number of pixels of the largest segment, p_{bare} (corresponding to the freestanding film, i.e.,

A_{bare}), were counted. This was then subtracted from the total number of pixels, p_{tot}, and divided by the same to calculate $\phi_{\text{f}} = (p_{\text{tot}} - p_{\text{bare}})/p_{\text{tot}}$. Processed images were visually compared against the raw data to verify satisfactory selection of algorithm parameters.

1.1.5 Solvent Vapor Assited SPD

A solutions of P3HpT was prepared at a concentration of 45 mg/mL and films were formed using 10 μL droplet volumes. Previously coated textured silicon was cleaned in chloroform, IPA, and DI water, followed by 30 minute air plasma clean. Solvent vapor treatment was performed in a recrystallization dish closed with a glass lid. A pool of chloroform was used at the source of vapor and the samples were elevated above the surface of the pool. The chloroform was preheated (60 °C) on a hotplate before the samples were added and was kept on the hotplate during vapor exposure, which lasted 10 minutes. To prevent chloroform condensation from forming on the lid and dropping onto the samples the lid was periodically heated with a heat gun. Samples were then cooled in liquid nitrogen before cleaving in order to facilitate brittle fracture of the P3HpT.

1.1.6 Co-solvent Assited SPD

Solutions of DIO in chlorobenzene were prepared based on premixed solvent volumes. DPP-DTT solutions were prepared at concentrations of 6 mg/mL of mixed solvent volume. Films were made using 10 μL droplet volume. Previously coated textured silicon was cleaned in chloroform, IPA, and DI water, followed by 30 minute air plasma clean. After transfer, samples were subjected to a solvent vapor treatment (60 °C, 10 min). To prevent chloroform condensation from forming on the lid and dropping onto the samples the lid was periodically heated with a heat gun.

1.1.7 Heat Assisted Experiment

A solution of P3HpT was prepared at a concentration of 10 mg/mL. Previously coated textured silicon was cleaned in chloroform, IPA, and DI water, followed by 30 minute air plasma clean. Films were prepared using 9 uL droplets. Samples were then either allowed to coat in ambient conditions (22 °C) or placed on a heated aluminum surface, which had a surface temperature of 69 °C, as measured using a thermocouple probe. All samples were filmed during the coating process, the footage of which was used to extract the time to coating completion.

1.1.8 Surface Energy Measurements

Contact angle measurements were done on planar P3HpT and plasma treated <111> silicon using a rame-hart goniometer (Model 290) using DI water and diiodomethane. Surface energies were calculated using using the OWRK method[39] for the plasma treated silicon (assuming a contact angle of 0° for water due to complete wetting) and the Wu method[40] for P3HpT. The interfacial energy was estimated using Girifalco and Good theory[41], assuming an interaction parameter, $\Phi = 1$.

1.2 Additional Information

1.2.1 Materials

Unless otherwise noted, all materials are commercially available and were used without further purification.

Polymers: PBTTT-C14 (Lot MKCH9345) and P3BT (regioregular, Lot MKBD6215) were purchased from Sigma-Aldrich. P3PT (regioregular, Lot SHK8-70) and P3HpT (regioregular, Lot SHK8-88) were purchased from Rieke Metals. P3HT (95.7% regioregular, Batch M102), DPP-DTT ($M_w = 278781$, Batch M315), and PTB7-Th ($M_w = 47043$, Batch M263) were purchased from Ossila.

Other Materials: Chlorobenzene (HPLC grade, 99.9%) and diiodomethane (ReagentPlus)

were purchased from Sigma-Aldrich. Chloroform (HPLC grade) was purchased from Fisher Chemical. DIO (Lot 2AM2E-IA) was purchased from Tokyo Chemical Industry. Silicon wafers (<100>, Czochralski Prime, 5-10 Ω cm, 525 ± 25 μm thick) were purchased from WaferPro. ITO coated pyramidal silicon was acquired from Sunpreme Inc.

1.2.2 Additional Figures

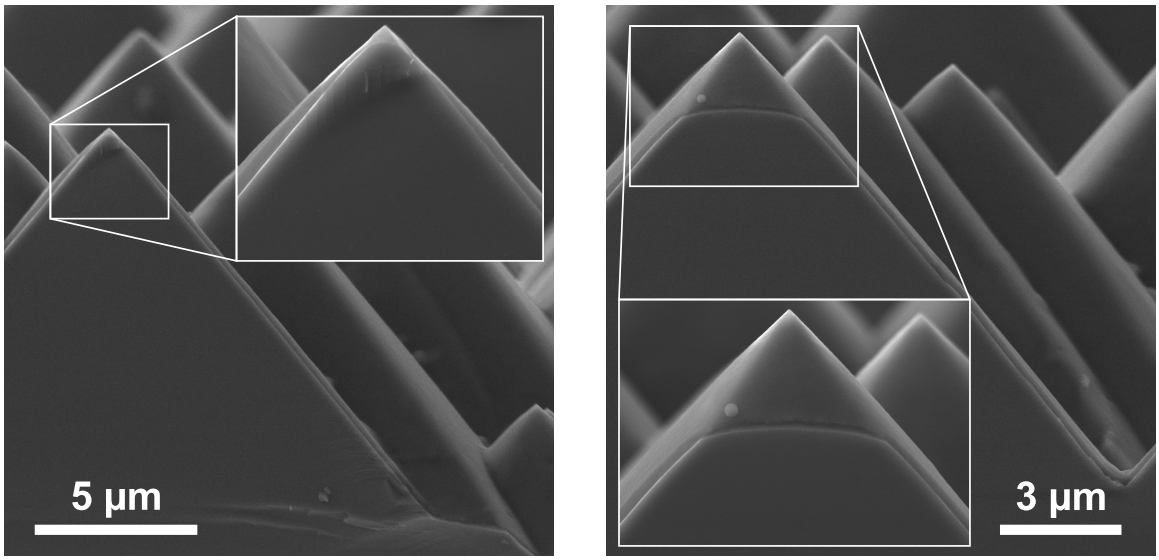

Figure 1.7. Scanning electron micrographs of silicon pyramids coated with P3HpT films after solvent vapor exposure, showing the thinning of the films near the apexes of the pyramids.

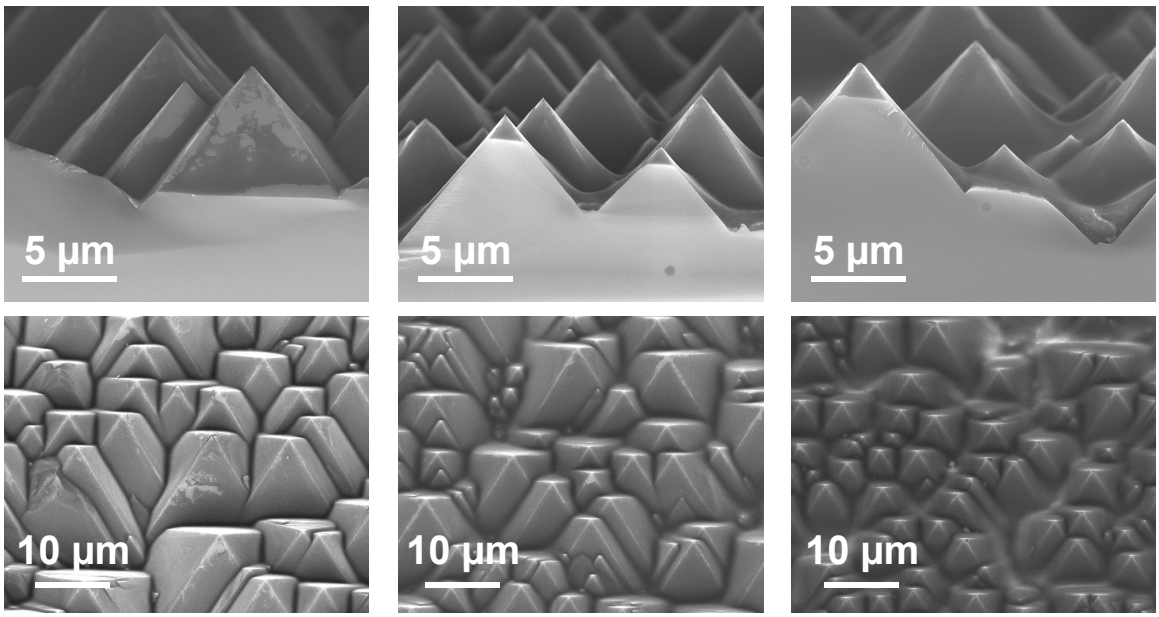

Figure 1.8. Micrographs of three spin-coated samples, shown from cross-sectional and angled perspectives. All samples were coated with a 500 RPM/s ramp up to 2000 RPM for 60 s. The concentration of P3HpT solution was varied between the samples. 10 (left), 30 (middle), and 50 (right) mg/mL each.

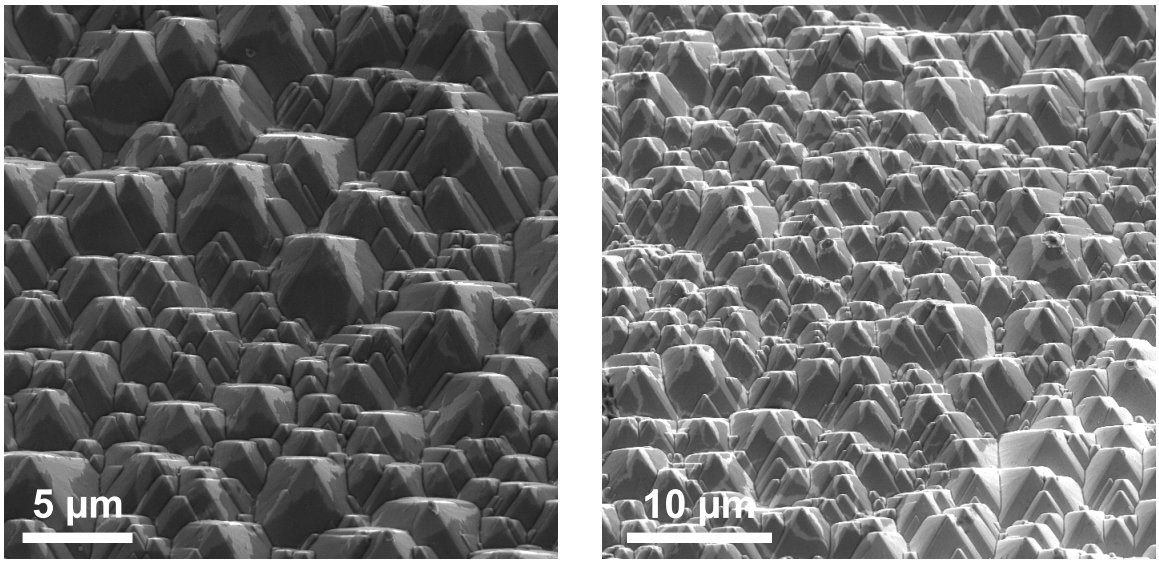

Figure 1.9. Scanning electron micrographs of ITO-coated pyramids covered with fractured PBTTT

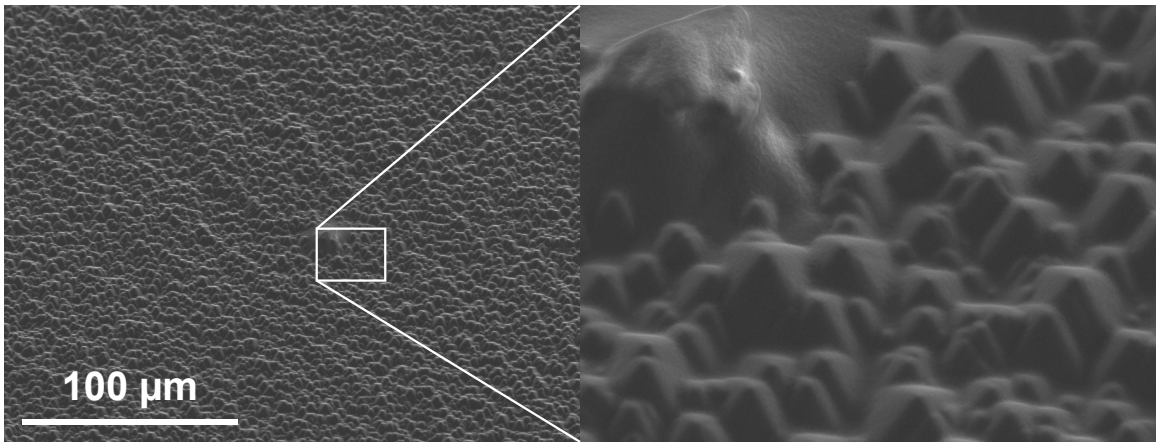

Figure 1.10. A BHJ film applied by SPD onto ITO-coated pyramids. Chloroform vapor was used to assist the coating process. The film was derived from P3HT:PCBM solution in chlorobenzene with 1% vol. DIO. The donor:acceptor ratio of the solution was 1:1, with a total concentration 30 mg/mL.

Chapter 1, in full, is a reprint of the material as it appears in ACS Materials Letters 2021. Guillermo L. Esparza, Darren J. Lipomi, ACS Press, 2021. The dissertation author was the primary investigator and author of this paper.

Chapter 2

Solvent-free Transfer of Freestanding Large-Area Conjugated Polymer Films for Optoelectronic Applications

2.1 Introduction

The ability to deposit thin films (< 100 nm) with precise thicknesses and in a sequential order is a critical aspect of semiconductor device manufacturing. As modern optoelectronic devices continue to incorporate more organic components (e.g., OLEDs), new processes are necessary that are compatible with a wide variety of hard and soft materials. In particular, there is demand for methods that yield homogeneous films on large substrates (>100 cm^2) that are compatible with previously deposited layers that may be sensitive to stressors such as heat, solvents, or other conditions.

Conjugated polymeric materials—defined by the delocalization of electrons through an extended system of π bonds—are of potential value in many such multi-layer devices, such as organic and hybrid perovskite photovoltaic cells. However, deposition of polymeric materials is generally limited to processing from vapor, liquid, or solution phases (e.g., chemical vapor deposition, spin-coating, or various printing methods). These classes of approaches have particular limitations. In the case of vapor-phase processing, the most significant drawback is that the monomers must be polymerized in situ in a reactive process (as in chemical vapor

deposition of polymers)[10,30,42]. This requirement restricts the structural diversity that can be achieved. For solution-phase processing, perhaps the most significant limitation is ensuring the solvents used do not damage the underlying layers—i.e., "solvent orthogonality." Deposition of pre-solidified films has been shown to open up new processing opportunities such as avoiding solvent incompatibility[43] or conformally coating textured structures[3].

Freestanding polymer films have been of significant scientific and technological interest over the last two decades, where they are used in service of fundamental studies and characterization[44–47], energy storage[48], sensing[49,50], separation membranes[51], tissue engineering[52,53], and various other applications[54–57]. Here, we have made use of freestanding films to fully circumvent the concerns of solvent orthogonality by enabling deposition truly free of liquid solvents. We named this process "solvent-free transfer" (SFT). A key step in SFT is to generate ultra-thin, freestanding films, e.g., using the technique of interfacial spreading described by others[9,38,58,59]. These films can then be drawn up onto a planar or cylindrical frame, which supports the edges of the films by van der Waals forces. These films can then be transferred directly onto a variety of substrates that are either bare or coated with other layers in a device stack in a manner that is compatible with roll-to-roll manufacturing. While the polymers are originally formed atop a water bath, they are highly hydrophobic and can be dried (for example, by vacuum) prior to the transfer such that substrate is agnostic to the solvents used to form the film. We demonstrate that SFT has significant potential in depositing over large areas by forming and transferring free-standing films which are up to 10×10 cm^2 in area, with thicknesses of ca. 20 nm. These films are characterized by various techniques and compared against spin-coated controls. Finally, we demonstrate the viability of the films as the hole-transport layers (HTL) in small area (0.07 cm^2) perovskite solar cells (PSCs).

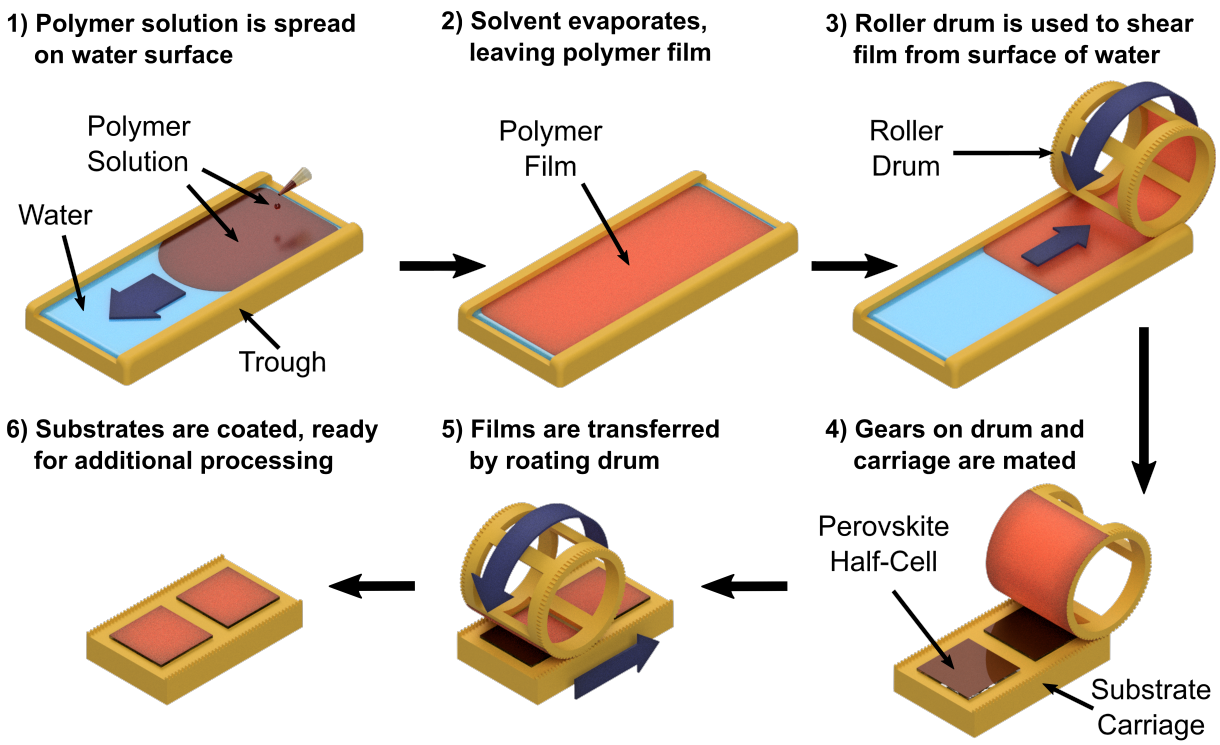

Figure 2.1. Summary of the solvent-free transfer process. A polymer film is formed on the surface of water before being sheared from the water surface using a cylindrical drum. The freestanding film can then be subsequently transferred to a solid substrate.

2.2 Results and Discussion

A summary of SFT, as it is applied in the fabrication of PSCs, is shown in Figure 2.1. The process begins by the interfacial spreading of a polymer solution on the surface of water held in a rectangular trough (step 1). The spreading of the polymer solution itself is driven by the Marangoni effect. Once the solvent evaporates, it leaves behind a polymer film suspended upon the surface of the water. The thickness of this film is determined by the concentration of the solution, the volume of the droplet, and the surface area of the trough (step 2). This film is then contacted at the edges by a supporting structure, in this case a cylindrical drum, to which the edges of the polymer film adhere. The drum is rotated to shear the polymer film off of the surface of the water (step 3). The drum with suspended films can then be aligned (step 4) and rolled over appropriately shaped substrates to transfer the film, e.g., to a perovskite half-cell (step

5). Once the films have been transferred, the device stack is ready for additional processing (step 6). Depending on the interfacial energies between the polymer and the desired substrate, the film will readily wet the substrate or it may benefit from additional treatment to promote complete contact. In the case of the perovskite/polymer pairings used in this work, we used chloroform vapor to promote the wetting process, but if the substrate surface is sufficiently hydrophilic, the wetting is rapid and effective. Footage of the film formation, drawing, and transfer using freestanding P3BT films (2.5 $\times$ 2.5 cm^2 in area, 20 nm thick) can be found in the Supplemental Video: Esparza_SFT_drum_setup.mp4.

In order to better assess the scope of SFT, we explored the survivability of films in the drawing step of the process, which we generally found to be the limiting factor. If a film could be drawn, then it could be transferred, but we did not find all films could be drawn. In our exploration, we found a variety of factors to play a significant role in the film survivability. These factors included intrinsic and extrinsic properties of the film (mechanical toughness and film thickness, respectively), as well as properties of the setup (the diameter of the roller drum). Conjugated polymers with high toughness were generally easy to draw. All of the P3ATs we tested had a toughness over 1.5 MJ/m3 and we were able to consistently draw films spanning a wide range of thicknesses, from approximately 15 nm to 135 nm. Higher thicknesses were not tested. On the other hand, DPP-DTT was the polymer we tested with the lowest toughness (approximately 0.15 MJ/m3), and we were never able to produce a high quality film with this polymer. All films drawn would fracture as the film was sheared from the water. A summary of the polymers (toughness and ease of drawing) with which we attempted to form freestanding films is shown in Figure 2.2a. Tensile test data gathered for this study can be found in Figure 2.9.

The most illuminating polymer we tested was PTB7-Th. We had two batches at our disposal that had dramatically different toughness, owing to their fracture strain, but similar tensile moduli and yield points. Representative stress vs. strain curves of the two batches are show in Figure 2.2b, as measured by the film-on-water method. The batches, referred to as ”57k” and ”47k” (based on their molecular weights) had approximate toughness of 1.8 MJ/m3 and 0.3

MJ/m3, respectively, which could be accounted for by the differences in their molecular weight, entanglement density, dispersity, or the presence of impurities. As expected, we were readily able to draw films made with 57k, but 47k was much more challenging. Using our typical drum diameter of 40 mm, no films were successfully drawn with 47k at a thickness of approximately 20 nm. However, increasing the drum diameter to 60 mm appears to alleviate the stresses the film is subjected to, and some films were successfully drawn at a thickness of 20 nm. We hypothesize this difference originates from the adhesion of water to the polymer as the film ascends when the drum is rotated. The water remains partially adhered to the film at first. With the smaller drum, the film is rapidly raised and is subjected to stresses as it is made to raise the water with it. By increasing the drum radius these stresses are reduced, as the film is more effectively sheared, rather than peeled, from the water surface. On the other hand, when the film thickness of 47k was increased to approximately 45 nm, we were able to draw high quality films with the 40 mm diameter drum. This increased survivability can be rationalized by considering that the stresses resulting from the drawing process (e.g., due to adhesion of the water) will be distributed over the greater thickness. This dilution of the stress reduces the maximum stresses, suppressing the formation and propagation of cracks.

Based on these results, we conclude that SFT is likely to be compatible with a broad range of polymers, but with some caveats. The toughness of the particular polymer and batch being drawn is a fundamental limiting factor. However, some strategies exist to mitigate the impact of the polymer toughness on the process. Here we explored the film thickness as well as the diameter of the rolling drum. The maximum thickness that can be produced using interfacial spreading, while retaining high film uniformity, is one factor that has not been well explored and that, in our experience, does vary between different polymers. The drum radius itself can be increased arbitrarily, keeping spatial restriction in mind. Beyond film thickness and increased drum radius, other strategies to expand the scope of SFT are expected to exist. Such strategies may pertain to the processing setup itself (e.g., other geometric aspects, drawing speed, and choice of liquid substrate) or polymer additives such as plasticizers which can alter the

mechanical properties of the film itself.

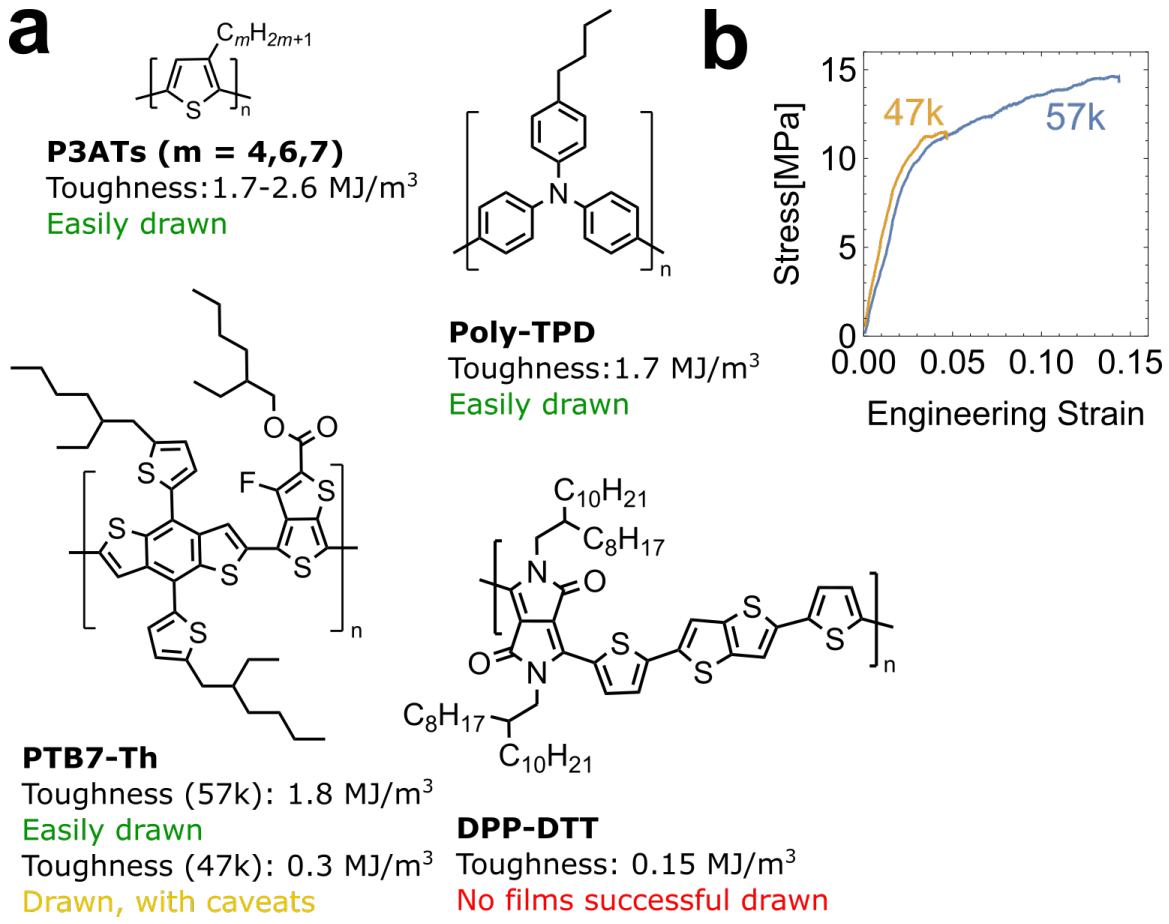

Figure 2.2. Chemical structures of the polymers with which we attempted to form freestanding films. Most could be readily drawn to form freestanding films. The 47 kDa batch of PTB7-Th required a larger drum radius or greater film thickness than other polymers. No freestanding films were successfully drawn with DPP-DTT. b) Characteristic stress vs. strain curves of the two PTB7-Th batches (57 kDa and 47 kDa) that were analyzed and drawn using SFT.

When forming large area films (100 cm^2), we replaced the rotating drum with a square planar frame (10 $\times$ 10 cm^2) which shears the film from the water surface by translating laterally on a linear bearing. This approach is conceptually equivalent to a roller drum of infinite radius. The use of the planar frame (instead of a large drum) is expected to minimize the strain on the film, and the drawn films were of high quality (Figure 2.3a). The film can then be transferred to a large area substrate by lowering down the film at a gentle, off-horizontal angle such that one corner touches down first. Upon contact with a high energy surface, such

as glass treated with air plasma, the film is quickly pulled down onto the surface as the triple interface (glass/polymer/air) propagates across the substrate. As this process evolves, air pockets sometimes form. We observed in most instances that these pockets deflated by themselves as the gas molecules diffused through the film, as was the case for the transferred film shown in Figure 2.3b. Otherwise, the elimination of the bubbles can be accelerated by exposing the substrate and film to solvent vapor.

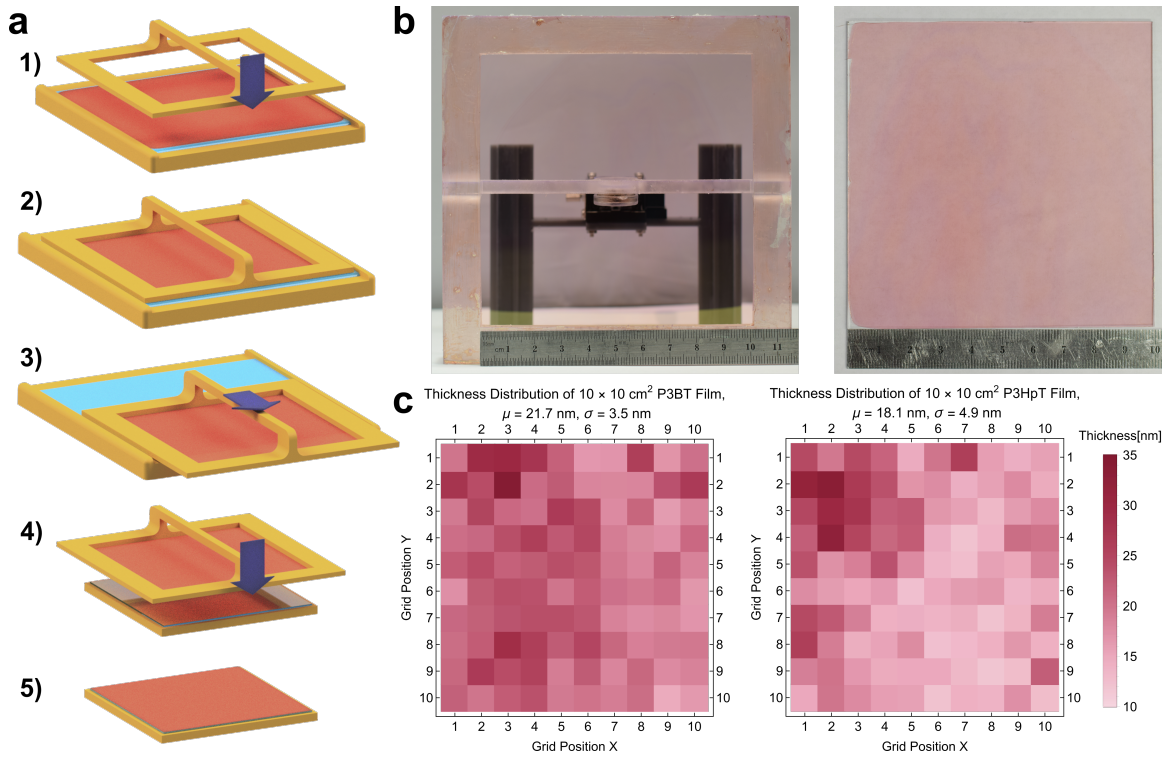

Figure 2.3. a) Summary of the large-area SFT variant, where the floating film is sheared off the water surface by a planar frame, which translates horizontally. This film can then be applied directly to a substrate. b) Photographs of a 10×10 cm^2 area film made of P3BT, mounted on the drawing frame (left) as well as after the same film was transferred onto a sheet of glass (right). c) Thickness measurements by profilometry of the same P3BT film (left) as well as a separate P3HpT film (right).

The thickness uniformity of these films was assessed by contact profilometry (see Figure 2.3c), which we found to have a reasonably low standard deviation (< 5 nm) for films with an approximate mean thickness of 20 nm. Additionally, the quality of the film formed also strongly depends on the local environment, control over which was limited in the ambient

laboratory environment. Factors such as the presence (or absence) of air currents can influence the uniformity of the film. Generally, the last regions to dry are also the thickest. This non-uniformity can be attributed to increasing concentration of polymer in the liquid region as the film solidifies in an adjacent region. Therefore, the manner in which the film dries can have a significant impact on the uniformity of the film. For example, in the case of large area films (which were formed with the setup simply placed in the open air of a fume hood), the last region to dry was consistently one of the back two corners, and when drawn, this region would be slightly, but visibly, thicker than the others. In contrast, when the evaporation was allowed to proceed in an enclosed container without flowing air, the overall solidification of the film was much less predictable, as was the subsequent non-uniformity. It may be possible to create a channel where uniform laminar flow can be leveraged to produce films with greater uniformity than is shown in Figure 2.3c.

We then measured the roughness and pinhole density of the films produced by SFT compared to those produced by spin-coating (SC). Films produced by both methods were of the same thickness (ca. 20 nm) and derived from the same solution. Atomic force microscopy (AFM) was used to generate a topographic map of the film surfaces before and after exposure to chloroform vapor, i.e. solvent-vapor annealing (Figure 2.4a). A quantitative look at the surface roughness of the films shows that, overall, the SFT films were slightly smoother than their SC equivalents (Figure 2.4b). As expected, the chloroform vapor treatment reduced the roughness for both the SFT and SC films. To ensure that the minima shown in the AFM images were not pinholes, we obtained scanning electron microscopy (SEM) images of the films (Figure 2.4c); no pinholes were observed.

In addition to AFM and SEM, we tested for the presence of pinholes using electrochemical chronoamperometry.[60] In this technique, we utilized a standard three-electrode system with 0.1 M tetrabutylammonium hexafluorophosphate (TBAH) in anhydrous propylene carbonate (PC) as the electrolyte and ferrocenne/ferrocenium (F_c/F_c^+) as the outer sphere redox couple. The films were held at 0.8 V vs. SHE for 30 seconds resulting in an exponential decay curve (Figure 2.4d).

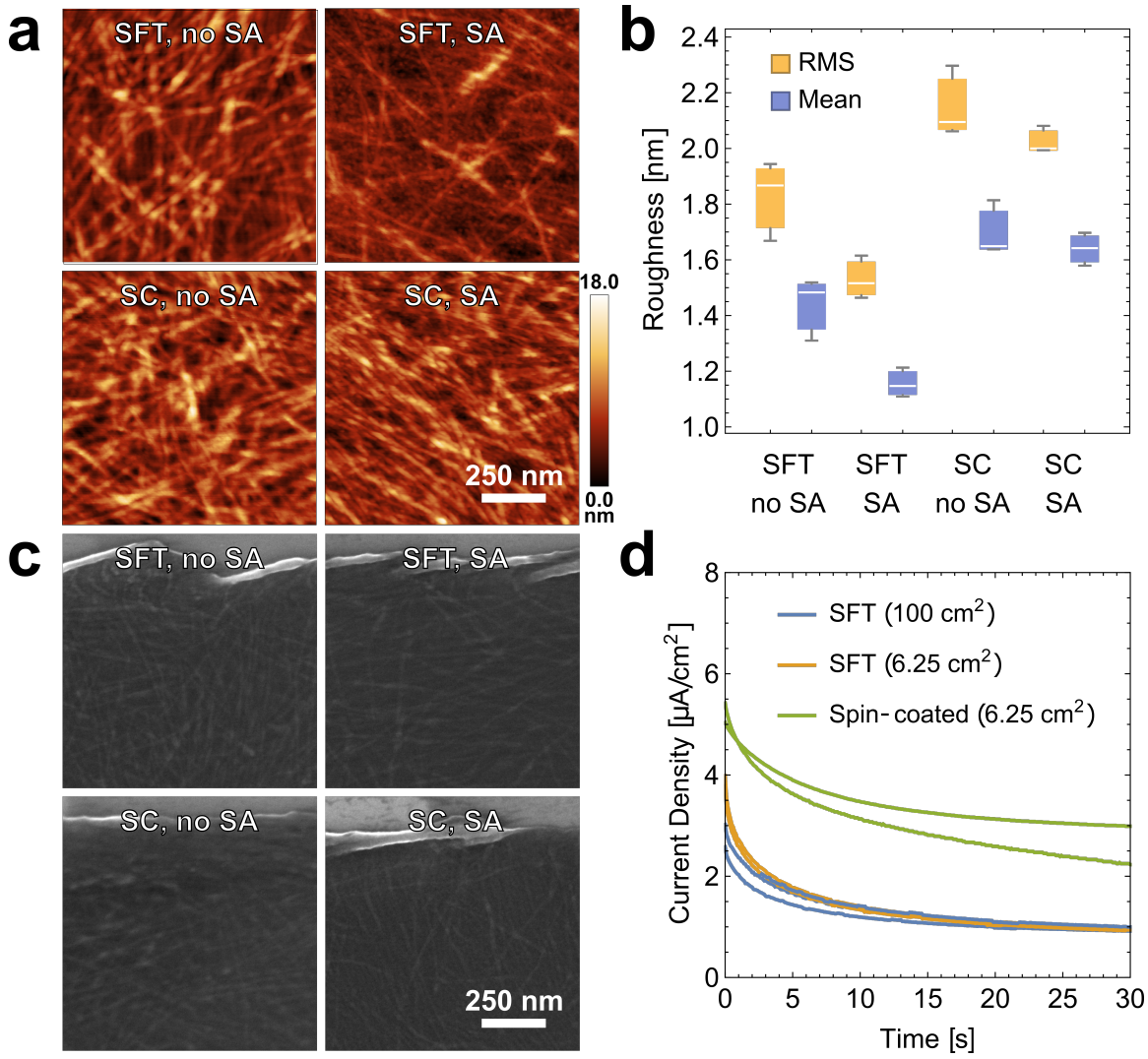

Figure 2.4. a) Atomic force microscopy of P3BT films that were deposited by SFT (top row) and spin-coated (bottom row). Films were evaluated before solvent-vapor annealling (SA) (left) and after SA (right). b) Root-mean-squared and mean roughness of the various films, before and after SA. c) Scanning electron micrographs of the same films. An InLens detecor was used to enhance contrast from surface roughness. The horizontal feature at the top of each micrograph is an intentionally scratched region to demonstrate the contrast between the polymer and its underlying silicon substrate. d) Electrochemical chronoamperometry of P3BT films that were deposited by large-area SFT (blue), small-area SFT (yellow), and spin-coating (green) To compare the scalability of SFT, multiple small area films are compared to multiple regions of a single large area film.

As detailed in our previous work,[61] the ratio of the current density as time approaches zero between the P3BT-coated ITO electrode and the bare ITO electrode (Figure 2.10) approximates the pore density by with charge can be transported whether by defects, pinholes, conductive

filaments, and impurities. Using this method, the surface coverage for films transferred by both SFT methods (small and large area) as well as SC controls was estimated. We find that all of the films performed similarly with the large area SFT, small area SFT, and SC films exhibiting 97%, 96%, and 95% coverage, respectively. The large area SFT films all came from a single film that was simultaneously applied to several small area (25×25 mm^2) substrates. All of these films were produced from the same sequentially filtered solution (0.45 μm and 0.2 μm pore sizes) and made in a Class 100 cleanroom in order to minimize the occurrence of pinholes.

Ultimately, we were interested in how films deposited by SFT perform in devices in comparison to films produced by spin-coating. In a typical perovskite solar cell (PSC), the absorber is sandwiched between two charge selective layers (the electron- and hole-transporting layers, ETL and HTL). In general, the selective layers must exhibit high electronic conductivity for the desired charge carrier, have favorable band alignments with the absorber, be chemically compatible with the absorber, have a high degree of stability against operational stressors, be optically transparent, and form interfaces with low levels of carrier traps. We reasoned that PSCs would be a good platform on which to test the viability of SFT of a conjugated polymer due to the lack of liquid solvents needed for SFT, which might otherwise damage the underlying perovskite absorber[62,63]. Additionally, the stability of PSCs is often further negatively impacted by the additives incorporated into the other layers in the device stack, such as the dopants used in the hole-transport layers (HTLs) made from small-molecular (non-polymeric) organic semiconductors.

We made PSCs with a variety of P3ATs, and found the electronic performance of all P3ATs tested to be comparable, with a slight loss in V_{oc} with increasing side-chain length. Ultimately, we settled on poly(3-heptylthiophene) (P3HpT) due to the favorable adhesion that we observed with the perovskite and this polymer, as opposed to that of glassier P3ATs with shorter alkyl chains. These films had free-standing dimensions of 2.5×2.5 cm^2, though the device active area was significantly smaller, at 0.07 cm^2, as defined by a stencil mask. Our findings are summarized in Figure 2.5. In general, we found the performance of the SFT films to

be comparable to the SC ones. The open-circuit voltage, V_{oc}, of SFT devices were somewhat lower, and showed greater hysteresis, when compared to those made with SC. However, the SFT devices displayed slightly increased short-circuit current density, J_{sc}, in both scan directions. The fill-factor (FF) was comparable between the two types of devices, with SC slightly outperforming SFT in the forward scan, but the opposite in the reverse scan. The underlying cause for these differences is unclear, but one possible explanation could be the difference in microstructure of the polymer which results from different processing conditions[1]. For example, the preferential edge-on microstructure of films formed by interfacial spreading when compared to films formed by SC could slightly alter the energetics at the HTL/perovskite interface, therefore affecting the photovoltaic metrics.

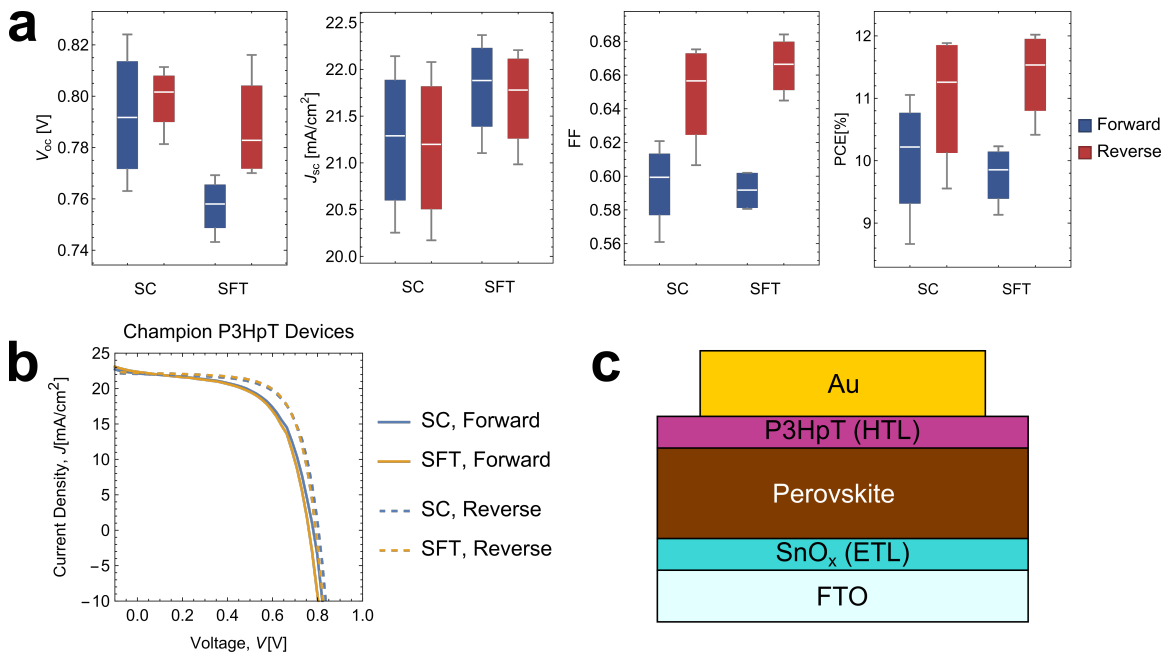

Figure 2.5. a) Photovoltaic metrics of perovskite solar cells using a P3HpT hole-transport layer deposited by solvent-free transfer (SFT) or spin-coating (SC). b) JV curves of the champion devices made using the two different deposition methods. c) Architecture of the device stack.

2.3 Conclusions

In summary, we have introduced a novel processing method, SFT, that leverages the mechanical robustness of conjugated polymers to form exceptionally thin, freestanding films that can be transferred onto sensitive substrates without using liquid solvents. The scope of the process was explored by attempting to utilize it to form films from a variety of conjugated polymers. Most polymers were quite compatible, but we identified toughness as a critical material property in determining the applicability of SFT with a particular polymer. The process was also demonstrated to be amenable to large areas, and the quality of the films is assessed for uniformity by profilometry (where we found films of ca. 20 nm thickness to have a standard deviation in thickness of 5 nm or less). The films were also compared against spin-coated controls. Film roughness was assessed using SEM and AFM (where we found SFT films to be slightly smoother than the controls), surface coverage was estimated by chronoamperometry (where SFT films yields slightly better coverage than the controls.) Lastly, we implemented SFT to produce the HTLs in PSCs, which performed very comparably to those in which the HTL was fabricated by spin-coating.

In SFT, after original solidification from solution, the subsequent processing occurs in the solid phase, allowing for deposition which is free of liquid solvents and therefore fully circumvents the usual need for solvent orthogonality. In principle, SFT could work with any polymer film that is floating on the surface of water or an alternative solvent, and interfacial spreading may be the most scalable method to produce such a film[38]. Additionally, because the polymers are initially processed from solution, SFT is expected to be compatible with the vast majority of conjugated polymers in use today. We believe this process holds additional potential in roll-to-roll application as well as in enabling other processing opportunities which leverage the ability to modify the film before applying them to the desired substrate.

2.4 Experimental Methods

2.4.1 General

All polymer solutions were made with chlorobenzene as the primary solvent, were magnetically stirred for >12 hours at approximately 60 °C, and were taken off the heat shortly before experiments and allowed to cool to room temperature. Air plasma treatments were done using a RF plasma cleaner from Harrick Plasma. The plasma cleans were done at 30 W with a chamber pressure of approximately 300 mTorr. All depositions on glass were done within 1 hour after plasma treatment.

2.4.2 Preparation of the Freestanding Polymer Films

All film formations and drawing were performed on custom-built systems. All custom parts, such as roller drums, troughs, and substrate carriage were printed on a Form 3 SLA printer using Form Clear Resin. The troughs in particular were treated in air plasma for an extended period of time (>3 hr) to crosslink the print surface and minimize leeching of the monomers and oligomers into the water used for interfacial spreading. Furthermore, a hydrophobic silane treatment was applied to the trough surface to modify the water contact angle and planarize the water surface in order to avoid pooling of the polymer solution.

2.4.3 Mechanical Properties of Polymers

The mechanical properties of the P3ATs were cited from[1]. All other mechanical properties were measured using the psuedo-freestanding "film-on-water" tensile test, which has been described elsewhere[64]. All reported mechanical properties were from films prepared by interfacial spreading, and all gathered data can be found in Figure 2.9.

2.4.4 Polymer Film Characterization

Profilometry: The initial thickness of transferred films was estimated by using the same "spreading parameters" (drop volume, polymer solution concentration, and dish size) to form

films which were transferred to planar (glass) substrates. For P3HpT and P3BT films, the concentrations used were 10 mg/mL and 7 mg/mL respectively. For the "small-area" trough (4 $\times$ 11 cm area) a droplet volume of 15 μL was used. For the "large-area" trough (13.5 $\times$ 15.5 cm area) a droplet volume of 70 μL was used. The thickness of these films was then measured using a Dektak XT profilometer.

Electrochemistry: For all electrochemical measurements, we used a standard three-electrode system with a bare/coated ITO as the working electrode, a platinum (Pt) wire was used as the counter electrode, and a non-aqueous single junction silver (Ag) reference electrode (Pine Research, AKREF0033) filled with 10 mM of silver nitrate in acetonitrile. For both cyclic voltammetry and chronoamperometry, the electrolyte used was 0.1M tetrabutylammonium hexafluorophosphate (TBAH, supplied by Fluka) in anhydrous propylene carbonate (Sigma Aldrich) where 20 g/mL of ferroene was added to serve as the redox couple. All voltages reported were corrected with 85% automatic and 15% manual iR compensation and all electrochemical measurements were performed on a Biologic VSP 300 potentiostatic with EC-lab software. The reference electrode was calibrated using the ferrocene/ferrocenium redox couple whose redox standard potential in propylene carbonate has been determined to be 0.624 V vs SHE.[65] In cyclic voltammetry, the films were scanned 5 times at which point they stabilized with minimal differences between scans 4 and 5. The scan rate was 20 mV/s. In the chronoamperometric measurements to determine pore density, the films were held at 0.8 V vs. SHE for 30 seconds after a 2 second linear sweep from open-circuit voltage. In order to minimize the formation of pinholes, all samples were prepared in a Class 100 cleanroom using a sequentially filtered P3BT solution (0.45 μm and 0.2 μm pore sizes).

Atomic Force Microscopy: The polymer films were deposited by SFT or spin-coated onto polished silicon which had been rinsed in acetone, ethanol, isopropyl alcohol, and deinonized water, followed by treatment with air plasma. AFM measurements were taken using a Veeco atomic force microscope (AFM) in tapping mode and analyzed using Nanoscope and Gywddion software.

Scanning Electron Microscopy: SEM micrographs were captured on a Zeiss Sigma 500 SEM with an accelerating voltage of 3.00 kV and an InLens detector. The samples used were the same as AFM.

2.4.5 Preparation of Perovskite Solar Cells

Substrate Preparation: Indium tin oxide (ITO) substrates were purchased pre-diced and pre-etched from Biotain Crystal Co. (TEC 8, 6-8 Ω/sq). They were cleaned by a series of sonication and washing steps as follows: sonicate in 2 vol% Hellmanex III in DI water for 15 min, rinse with DI water, sonicate in DI water for 15 min, rinse with DI water, sonicate in IPA (99.5% purity) for 15 min, rinse with IPA, sonicate in acetone (99.9% purity) for 15 min, rinse with IPA, and then dry with filtered dry air. Immediately prior to tin oxide deposition, the FTO substrates were UVO-treated for 20 min.

Tin Oxide Electron Transport Layer: The seed solution was prepared by diluting a colloidal dispersion of SnO_2 (15% in water, Alfa Aesar) with DI water (Alfa Aesar) in a 1:4 volume ratio. Prior to use, the solution was stirred at room temperature for 4 hours then filtered with a 0.22 μm PTFE filter. Cleaned and UVO-treated substrates were prepared and 150 μL of the SnO_2 seed solution was spun atop the substrates at 4000 RPM for 30 seconds in air. The films were then sintered at $150 for 30 minutes also in air.$

Perovskite Absorber: The selected perovskite composition has a nominal solution stoichiometry of $FA_{0.78}MA_{0.05}Cs_{0.17}Pb(I_{0.85}Br_{0.10}Cl_{0.05})_3$ dissolved in a 3:1 v/v mixture of DMF and DMSO at a 1.25 M concentration. Prior to the perovskite deposition, the tin oxide coated ITO substrates were treated again with UVO to improve the wettability of the perovskite solution resulting in better films. The films were spin-cast at 5000 RPM for 50 s with a 200 μL drop of methylacetate 22 s into the spin. The resulting films were annealed at 100 °C for 30 min. All perovskite processing was conducted in a nitrogen-filled glovebox.

FAI was purchased from GreatCell Solar Materials, CsI (99.999% purity) and MACl (99.0% purity) from Sigma Aldrich, lead iodide (99.99% purity) and lead bromide (99.99%

purity) from TCI, and lead chloride (99.999% purity) from Sigma-Aldrich.

P3AT Hole Transport Layer: Both poly(3-heptylthiophene) and poly(3-butylthiophene) were dissolved in chlorobenzene at a concentration of 10 and 7 mg/mL, respectively. In the case of the solvent-free transfer, a droplet of solution, with a volume of 15 μL, was dropped onto water in a narrow trough and allowed to solidify on top of the water. The film formation and drawing was done in an oxygen-free, nitrogen-filled glovebox with an oxygen content below 0.02%. The films were then transferred into a separate nitrogen-filled glovebox ($<$ 1 ppm water or oxygen), with a drying step in the antechamber under dynamic vaccum for 10 min. The films were then transferred onto the perovskite device stack and conformal coating was promoted by a vapor treatment of chloroform, performed in a recrystallization dish with a glass lid, at room temperature, for 5 min.

Gold Top Contact: A 100 nm layer of gold was deposited by vacuum thermal evaporation with a 5 nm adhesion layer deposited at 0.03 Å/s then finshed at 0.5 Å/s.

JV Testing: After device fabrication was completed, the cells were allowed to age in nitrogen for 15 days, as this was observed to significantly improve the device fill factors by eliminating "double-diode" behaviour in the JV sweeps (Figure 2.14). Devices were tested in nitrogen environment using an ABET Mondel 11002 SunLite Solar Simulator, under AM 1.5G, at 100 mW/cm^2, with a scan speed of 0.1 V/s, and a fixed aperture of 0.07 cm^2. Prior to testing, the light intensity was calibrated using a standard silicon reference cell purchased from PV Measurements, Inc.

2.5 Additional Information

2.5.1 Discussion on Interfacial Spreading

Because of the likely reliance of SFT on interfacial spreading, it is important to assess the limitations and unresolved challenges of the latter, as it is may be the limiting factor in the implementation of SFT. For reasons we do not fully understand and which, to our knowledge,

have not been explored in the literature, there is substantial variability in the polymers that will form a high quality film. Batch to batch variation, in particular, seems to play a significant role. Of the various P3HT batches that we used, only one of them formed highly uniform films. The rest of the batches tended to form films which had significant thickness variation across lateral length scales on the order of mm to cm. Interestingly, all of the other batches of P3ATs used formed highly uniform films. Similarly, we were able to form high quality films with one batch of Poly-TPD, but not another that we tried, which resulted in wrinkled films as the solvent evaporated. For comparison, both of the PTAA batches that we tried, which has a very similar structure to Poly-TPD, did not form high quality films. This suggests the presence of solubilizing side-chains may also play a role in facilitating the film formation. Therefore, to our knowledge, the specific properties which allow a given polymer and batch to spread effectively remains an open question.

Because we exclusively used interfacial spreading to form the floating films, this means we only used polymers with which we were able to form high enough quality films. For reasons we do not fully understand and which, to our knowledge, have not been explored in the literature on interfacial spreading, there is substantial variability in the polymers that will form a high quality film. However, batch to batch variation seems to play a significant role. Of the various P3HT batches that we used, only one of them formed highly uniform films. The rest of the batches tended to form films which had significant thickness variation across lateral length scales on the order of mm to cm. Interestingly, all of the other batches of P3ATs used formed highly uniform films. Similarly, we were able to form high quality films with one batch of Poly-TPD, but not another that we tried, which resulted in wrinkled films as the solvent evaporated. For comparison, both of the PTAA batches that we tried, which has a very similar structure to Poly-TPD, did not form high quality films. This suggests the presence of solubilizing side-chains may play a role in facilitating the film formation, though batch-to-batch variation is also clearly playing a role. Therefore, to our knowledge, the specific properties which allow a given polymer and batch to spread effectively remains an open question that will need to be eventually resolved

if SFT is to have viability in any sort of high throughput implementation.

Additionally, water is not the only liquid that can be used to form interfacially-spread films, but it was the one that produced the highest uniformity films in our exploration. In seeking alternatives to water we particularly looked for liquids with a high surface tension that are immiscible with chlorinated solvents. We found propylene carbonate, ethlylene glycol, and glycerol could all be used to produce interfacially spread films, but the films produced all had inferior uniformity to those produced on water or produced films which were discontinous/fractured over the length scales desired for the SFT process. It is possible other liquids, such as molten gallium or mercury could also be used, though we had issues with the gallium oxidizing and chose not to use mercury due to its toxicity.

2.5.2 Additional Figures

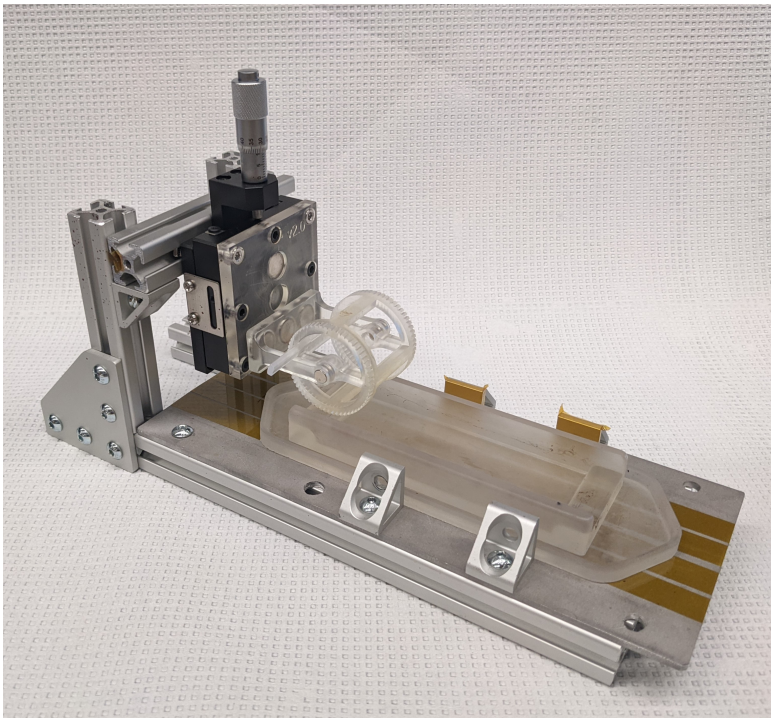

Figure 2.6. The setup used to draw the small area (25 $\times$ 25 mm) freestanding films.

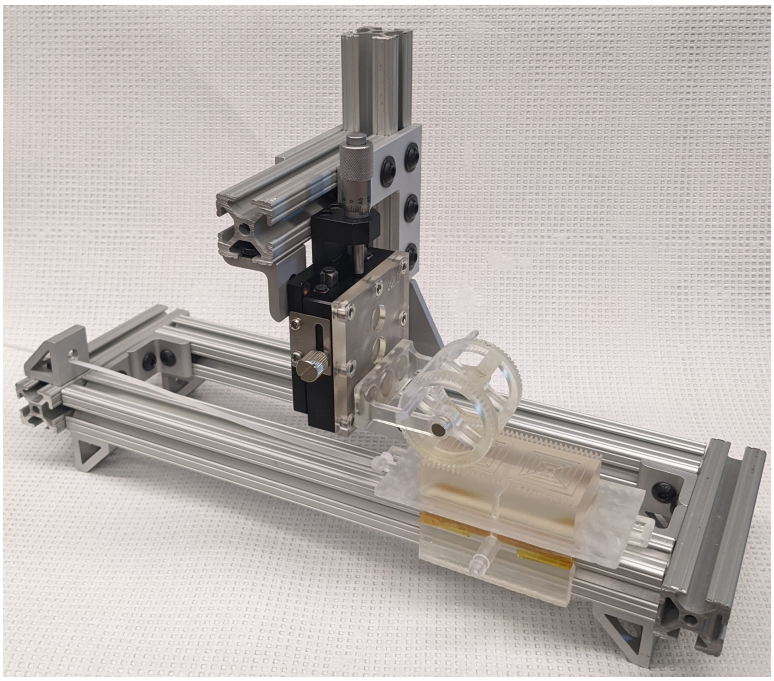

Figure 2.7. The setup used to transfer the small area (25 $\times$ 25 mm) freestanding films onto correspondingly sized substrates. Note the presence of a vacuum line on the carriage to hold the substrates in place as the transfer is performed.

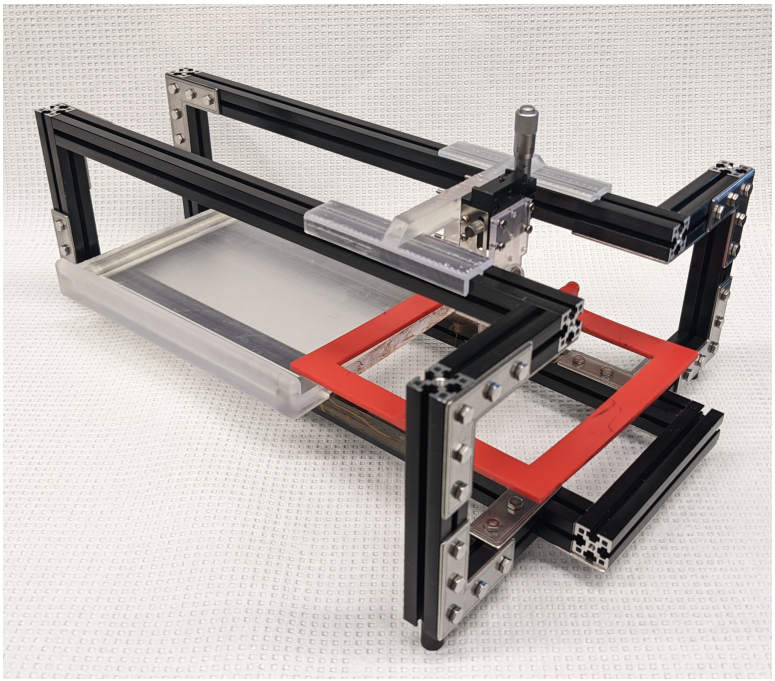

Figure 2.8. The setup used to draw and transfer the large area (10 $\times$ 10 cm) films onto correspondingly sized substrates. The setup is shown in the drawing configuration. The transfer configuration requires the trough be swapped out for a substrate holder, but is otherwise the same.

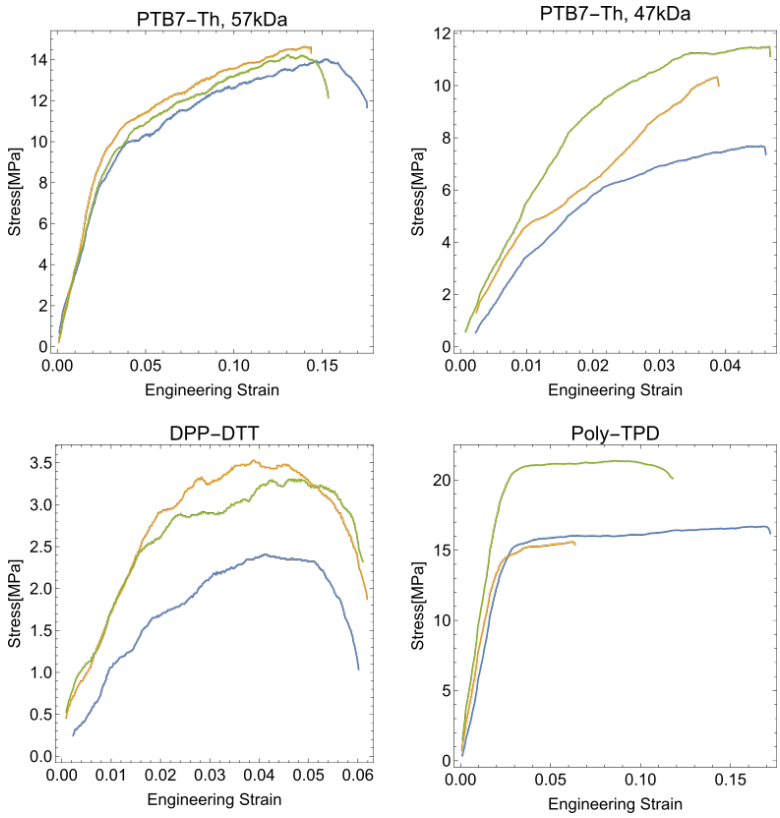

Figure 2.9. The data gathered by pseudo-freestanding tensile tests (”film-on-water” method) for this study. All films were formed by interfacial spreading.

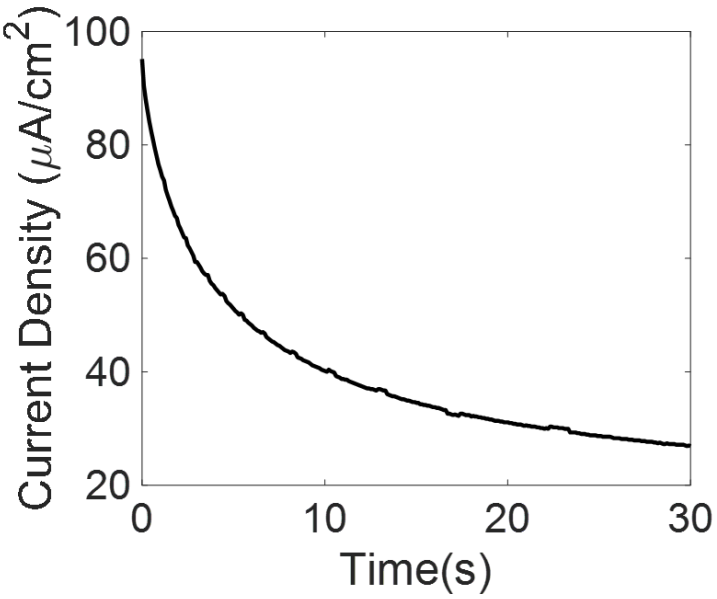

Figure 2.10. Chronoamperometry of the bare ITO substrate.

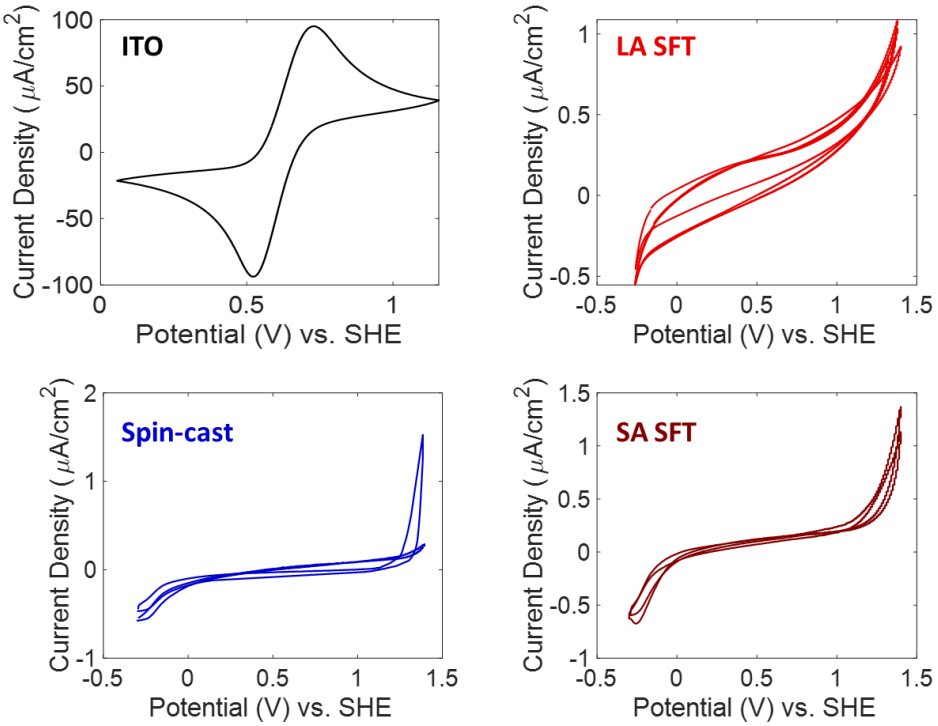

Figure 2.11. Cyclic voltammograms of each set of films including the bare ITO (black), spin-cast P3BT atop ITO (blue), large area SFT atop ITO (light red), and small area SFT atop ITO (dark red).

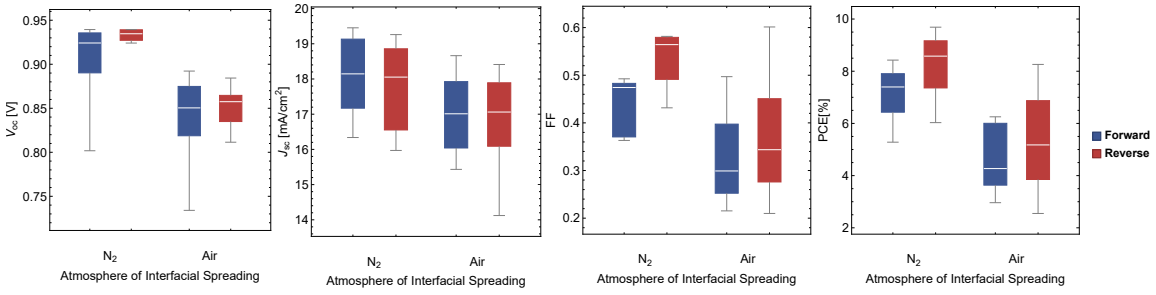

Figure 2.12. Photovoltaic metrics of perovskite cells using an SFT P3BT hole-transport layer, where the atmosphere used during film formation was either ambient air or N_2

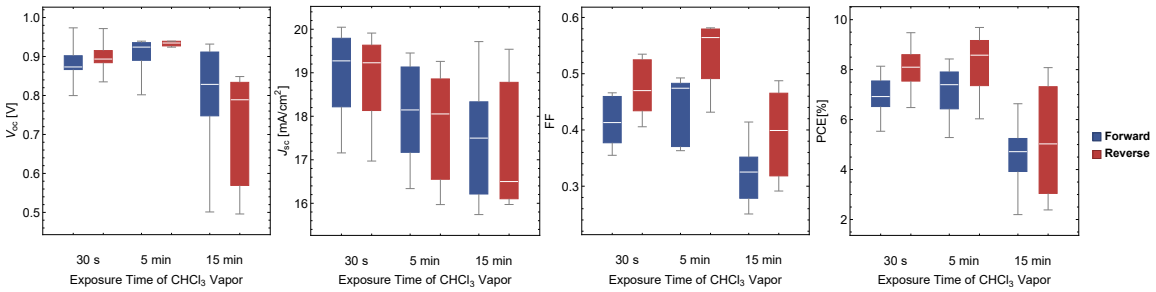

Figure 2.13. Photovoltaic metrics of perovskite cells using an SFT P3BT hole-transport layer, where the chloroform vapor exposure time was varied after the P3BT was transferred

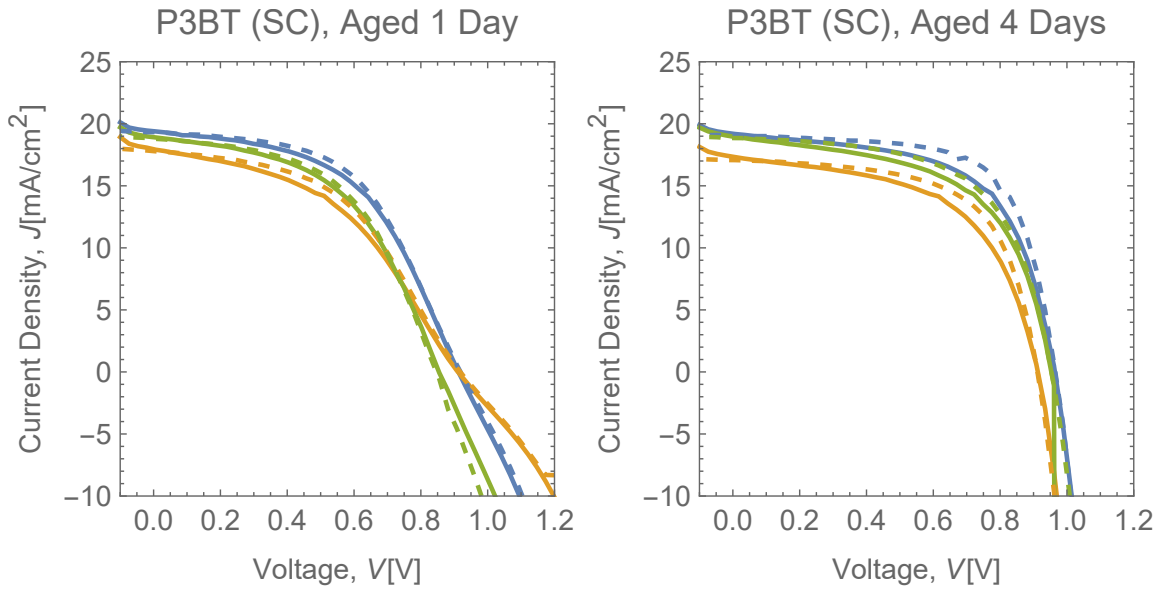

Figure 2.14. Current Density vs. Voltage sweeps of a batch of perovskite solar cells using spin-coated P3BT HTLs. The effect of aging in N_2 is shown to improve the fill-factor significantly as the "double-diode" behaviour is reduced/eliminated. This effect was consistent across P3AT batches, both for spin-coated films and those applied by SFT.

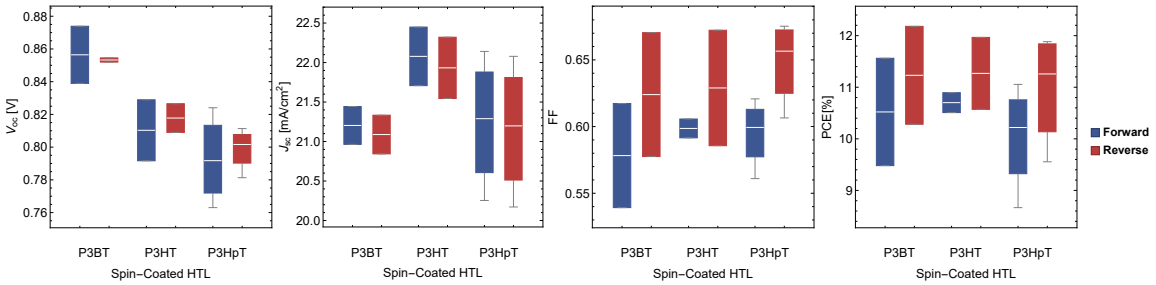

Figure 2.15. Photovoltaic metrics of perovskite cells using one of several spin-coated P3ATs as the HTL. While there is a trend towards higher V_{OC} for shorter alkyl side-chains, the generally comparable performance of the P3ATs, along with the improved wetting of P3HpT on the perovskite, led us to choose P3HpT as our HTL for subsequent batches.

Chapter 2, in full, is a reprint of the material as it appears in Advanced Materials 2023. Guillermo L. Esparza, Moses Kodur, Alexander X. Chen, Benjamin Wang, Jordan A. Bunch, Jaden Cramlet, Rory Runser, David P. Fenning, Darren J. Lipomi., Wiley Press, 2023. The dissertation author was the primary investigator and author of this paper.

Chapter 3

Circumventing Sputter Damage in Opto-electronic Devices by Mechanical Transfer of Freestanding Transparent Conductive Oxide Films

Many opto-electronic devices require the use of an electrode which is both optically transparent and electronically conductive. However, transparency and conductivity are two material properties that typically exist in opposition to each other. The mobile charge carriers that enable conductivity in a material are consequently also capable of responding to, and reflecting, the oscillating electric field of incident light. This relationship is evidenced by inspecting the equations for the plasma frequency,

$$\omega_p = \sqrt{\frac{ne^2}{\varepsilon\varepsilon_0 m}}, \tag{3.1}$$

and Drude conductivity,

$$\sigma = \frac{ne^2\tau}{m}, \tag{3.2}$$

where n, e, m, ε, ε_0, and τ are the carrier number density, electron charge, effective electron mass, dielectric constant, permittivity of free space, and mean free time between ionic collisions, respectively. While not a perfect comparison (as this is strictly a DC conductivity), we can see

how an increase in the carrier concentration increases both the conductivity as well as the plasma frequency, facilitating the transport of electric current, but also increasing the thresh-hold at which the material stops reflecting light (decreasing its transparency.)

Because of this oppositional relationship, the material options available which are both transparent in the visible spectrum but still highly conductive are very limited. While ultra-thin metal coatings and conducting polymers are possible options, the overwhelmingly most common choice in industry is some type of transparent conducting oxide (TCO). These materials are unique in that their reasonably wide bandgap and low plasma frequency allow them to be largely transparent across the visible spectrum while retaining conductivity approaching that of a true metal. However, such materials are stoichiometrically complex and so their deposition presents a variety of challenges[4].

Due to the variety of elemental species they contain, evaporative techniques are challenging routes of deposition for TCOs. The various components will have a range of vapor pressures and therefore the deposited film will tend to have a stoichiometry which is distinct from that of the source. Furthermore, the range of vapor pressures also means the stoichiometry of the source material itself will change as it is used. To counteract such effects, evaporation of TCO films typically require a reactive component, such as a low partial pressure of oxygen introduced during the process, to produce films at a desirable stoichiometry[66].

The overwhelmingly most common technique for thin-film deposition of TCOs is magnetron sputtering. In its most common form, magnetron sputtering simply entails striking a plasma with an inert process gas (such as Ar), with the plasma ions then made to strike a puck of the material to be deposited, called the sputter target. As the ions strike the target surface, they eject atoms from the target which then condense on the surface of the desired substrate. Unlike evaporative techniques, the composition of sputtered films can be carefully controlled by the ratio of powders used to press the sputter targets. While there can still be some variation in composition (due to differences in sputter yield for the various species) this variation tends to be much less significant than in films deposited by evaporation[4,5].

Despite its benefits, sputtering has its own set of drawbacks. Chief among them is the damage that is caused by the sputtered atoms on the surface of the substrate onto which they are deposited. While the kinetic energy of evaporated atoms tends to be less than 1 eV, kinetic energies of sputtered atoms are often as high as 100s of eV[4]. Such energies often result in implantation, bond breakage, dislocations, and other types of damage on the substrate surface. The aggressive nature of sputtering can impose significant process restrictions, particularly with the advent of functional yet sensitive materials, such as organic and hybrid (e.g. perovskite) semiconductors.

Because such damage can significantly impact the electrical performance of the substrate surface, the most common strategy to avoid sputter damage is to simply deposit the TCO before depositing any other active layers. It can be deposited on a variety of substrates, such as glass, and then the remainder of the device layers can be deposited, finishing with an electrode than be deposited by gentler means, such as evaporation. However, in certain cases it is impossible to start with the TCO. For example, in perovskite/perovskite or silicon/perovskite tandem photovoltaics, it becomes mandatory that a transparent but conductive film be deposited on a perovskite cell. In the case the perovskite/perovskite tandems this film serves as a recombination junction between the cells and in the case of silicon/perovskite tandems this layer is the top (sunny side) electrode. In both cases, the film must let in light but also be conductive to allow charge to be transported.

In cases like these tandem cells, if sputtering is to be used, the strategy most often employed to avoid sputter damage is to deposit some type of protective buffer layer. These layers are typically some type of metal oxide, such as SnO_x[7,13], WO_x[67], and VO_x[68,69], which are all wide-bandgap materials. In order to achieve the film densities required for an effective, yet thin, buffer layer, atomic-layer deposition (ALD) is employed. While effective, this technique is not generally considered to be highly scalable, and so there is a need to find alternatives to the current approach to device fabrication[70].

In order to become scalable, the "buffer layer" strategy leaves two options: either change the way the buffer layer is deposited such that it is more scalable while retaining desirable

properties, or change the way the TCO is deposited to reduce the amount of damage the sputtered atoms cause, allowing for a lower quality buffer layer. With respect to changing the deposition of the buffer layer, various methods have been explored, but among the most promising it "spatial-ALD" methods that attempt to increase the scalability of ALD to be in line with the rates necessitated by modern manufacturing lines[71]. Many alternative sputtering techniques for TCOs are also currently being explored[4], but in this work we present an altogether different approach. The TCO is deposited by conventional RF sputtering, but is initially deposited onto a "sacrificial" freestanding polymer film, completely separate from the rest of the device. This polymer film can be exceptionally thin (20 nm) and once the polymer/TCO bilayer has been formed, it can be mechanically transferred onto the desired substrate. This approach limits the sputter damage strictly to the freestanding film substrate, sparing all other layers in the stack from such damage. Depending on the subsequent processing route taken, this polymer film can either be incorporated into the device stack as a functional (e.g. charge selective) layer, it can be stripped from the freestanding structure (leaving behind a freestanding TCO film), or the bilayer can be flipped such that the polymer does not play an active role in charge extraction from the device. In this work we characterize these deposited TCO films in comparison with controls deposited on rigid substrates. We performed this characterization by UV-Vis spectroscopy to compare their optical properties and 4-point sheet-resistance measurements to compare their electrical performance. Finally, we incorporate the freestanding bilayer films into perovskite solar cells to serve as a sputter-free TCO contact.

3.1 Process Description

Formation of the freestanding TCO films begins with fabrication of the freestanding polymer substrate. A thin polymer film is formed on the surface of water via interfacial spreading of polymer solution[9]. The floating film is then sheared off the water surface while adhered

(via van der Waals forces) to a supporting frame. This approach has been demonstrated to be feasible in areas as large as 100 cm^2 [8]. Once the polymer film has been rendered freestanding on a supporting frame, the TCO can be sputtered directly on the freestanding film without further preparation. An angled cross-section of a freestanding bilayer film can be seen in Figure 3.1a, where the two films are beginning to de-laminate due to the tearing of the bilayer. Additionally, the freestanding film can be patterned with use of the shadow mask which is slightly spatially separated from the freestanding film such that contact with (and therefore damage of) the film does not occur. A film patterned with a TCO electrode can be seen in Figure 3.1b.

Sputter deposition onto the freestanding film does have some caveats. Importantly, arcing during sputtering becomes particularly deleterious. Arc discharge in sputtering, rather than the desirable glow discharge, results in transient and highly localized heating of the sputter target surface. This discharge results in pitting of the surface and an associate ejection of clumps of material. When depositing on a rigid substrate, arcing has negative impacts on film smoothness due to the presence of large particles which pepper the film mid deposition. However, when depositing on freestanding films, these particles can completely destroy the freestanding films. Numerous times during our process optimization we observed freestanding films collapse immediately after an arcing event. This occurrence was particularly prevalent when the arcing happened early on in the deposition. Presumably, once some TCO thickness has been built up, the bilayer structure stabilizes the freestanding films and they become more resilient to damage from ejected material. Ultimately, we found that with proper target care (i.e. slow power ramps of 10 W/min and limited power densities of 19 W/in^2) such arcing events could be significantly limited and the structural integrity of the freestanding films preserved.

Beyond the issues caused by arcing, as well as the damage intrinsic to sputtering, there are additional challenges that come with sputtering material on freestanding films. The most notable is an apparent increase in film area which leaves the overall bilayer film somewhat prone to wrinkling. Whereas the polymer film goes into the chamber taut and flat, the bilayer post deposition comes out somewhat slack and fluttery. This can be clearly seen in Figure 3.1b, where

the patterned region where TCO was deposited is visibly wavy, while the rest of the freestanding film remains taut as it was before it went into the deposition chamber. The exact cause of this wavy-ness is not completely clear, but we believe it is likely due to both heating of the polymer film, which makes it more compliant, and the pressure differential between the front and the back of the polymer film originating from the deposition itself. The main evidence for this hypothesis is the visible upwards bowing of the films during the deposition, which could be plainly observed the chamber window part way through the depositions, but which was not evident at the start, suggesting it was a deformation which had to be built up over the course of a given deposition.

This excess in area makes the films somewhat more difficult to transfer for two reasons. Firstly, achieving a clean wrinkle-free transfer with freestanding films requires that contact between the film and the substrate initiate at only one location, such that the wetting of the film on the surface can propagate out from that location. When the film is able to flutter, it becomes much more likely that the film will contact in multiple places. Additionally, the fact that this slack exists, while the contact perimeter with the frame remains the same, implies that there is now some curvature "frozen" into the film. Therefore, mapping this curved bilayer back onto a planar surface is impossible to do without some deformation (akin to the deformations that occur in map projections when making a planar map of our spherical world.) Both of these factors contribute to the occurrence of wrinkles in the transferred film, which has been a significant hurdle in carrying out this work.

Lastly, once a freestanding film has been created, transfer can, in principle be performed easily if the interfacial interactions between the film and substrate are favorable (i.e. if they lead to a reduction in interfacial free-energy of the system.) In our previous work this was plainly visible as large-area coatings (100 cm^2) could occur in fractions of a second once contact between the polymer film and substrate occurred. In transferring TCO/polymer bilayers, the wetting process is complicated by the stiffness of the oxide film, which limits the ability of the film to readily deform to wet a given surface, particularly if the substrate is not smooth, as is the case in perovskite films.

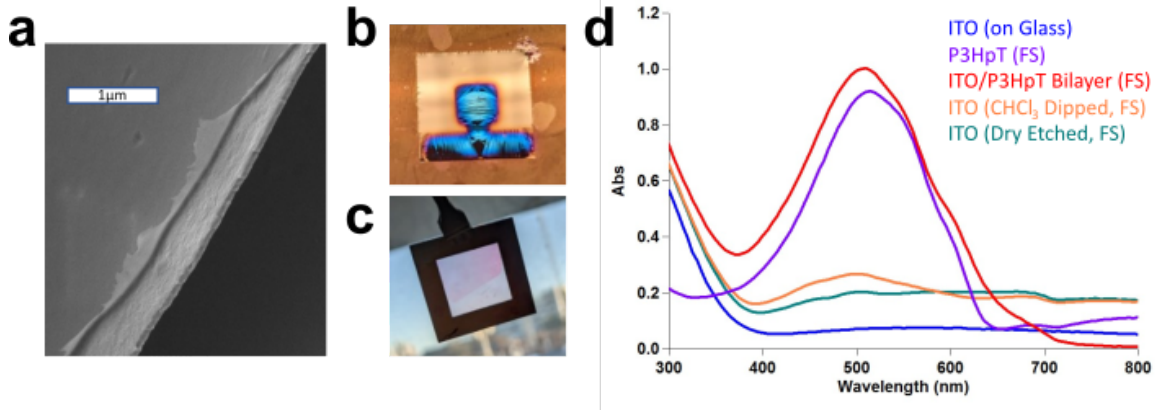

Figure 3.1. a) Scanning Electron Micrograph (SEM) of a freestanding bilayer film (P3HpT / ITO). The P3HpT is on the left and can be seen delaminating from the ITO due to the tear in the film. b) Freestanding P3HpT film which has been patterned with ITO by use of a spatially separated shadow mask. c) A freestanding bilayer film (P3HpT/ITO) which has been partially dipped in $CHCl_3$ to strip the ITO of the polymer. d) UV-Vis spectra of various freestanding films ITO sputtered on glass (glass signal subtracted). These freestanding films are composed of P3HpT, ITO/P3HpT bilayer, ITO after P3HpT dissolution in $CHCl_3$, and ITO after the P3HpT was dry etched in air plasma. All ITO was deposited in the same sputter process.

3.2 Characterization

In carrying out this work, we wanted to characterize the effect that sputtering on free-standing polymer films had, if any, on the TCO films. Additionally, we wanted explore options for removal of the polymer film such that we would be left with a truly freestanding TCO film, rather than TCO/polymer bilayer. We explored two methods of polymer removal from deposited indium-tin oxide (ITO) films, by either dipping in solvent ($CHCl_3$ for 1 minute) or dry etching in air plasma (20 minutes). We then took optical absorbance spectra of the freestanding films, having selected P3HpT as the polymer due to its strong optical signal. These spectra are compared against a neat freestanding P3HpT film (no ITO deposition) and ITO which was concurrently deposited on glass. A partially dipped film can be seen in Figure 3.1c and the absorbance spectra are shown in Figure 3.1d.

There are several notable features in the absorbance spectra. While the dry etching appears more effective at removing the polymer, there is clearly some residual polymer that

lingers, as evidence by the features around 500 and 700 nm. Interestingly, there is also a marked increase in apparent absorption beyond 650 nm after the polymer has been stripped. We do not believe this apparent increase to be indicative of true absorption, but rather an artifact originating from our UV-Vis spectrometer. Our instrument cannot distinguish between light that is reflected versus light that is truly absorbed. With the absence of polymer or glass, there is likely to be in increase in the mismatch of optical impedance on the backside and therefore an increase in the reflection of light. This is qualitatively supported by the fact that the freestanding ITO does visually appear much more reflective than the ITO that has been deposited on the glass.

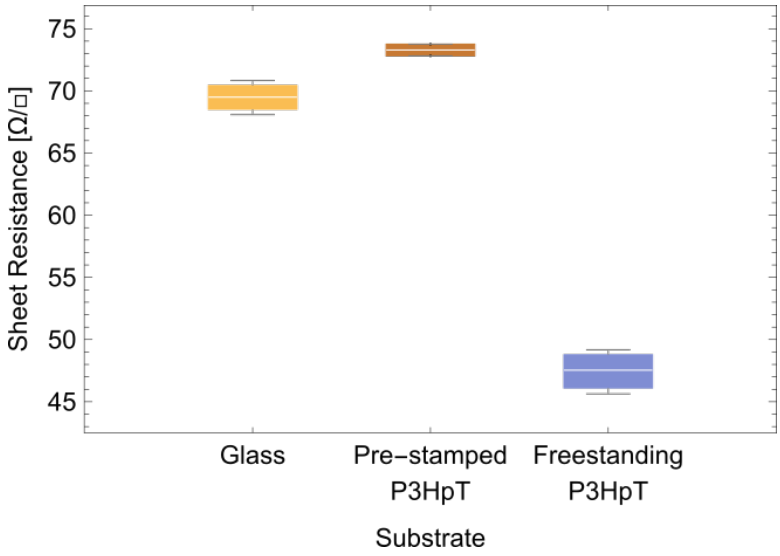

Figure 3.2. 4-point sheet resistance measurements of ITO deposited directly on glass, on P3HpT which had been pre-stamped on glass, as well as on P3HpT which was freestanding during deposition and subsequently transferred onto glass. All ITO was deposited in the same sputter process.

We used 4-point sheet resistance measurements in order to asses the electronic impact that depositing on freestanding films might have on the ITO as compared to depositing directly on glass or on polymer which had been pre-stamped on glass. For this experiment the freestanding bilayer was transferred onto glass before measurement, all ITO was deposited concurrently, and we, again, used P3HpT as the polymer of choice. The results are shown in Figure 3.2. Interestingly, there was a significant decrease in the sheet resistance of the samples deposited on

the freestanding films when compared to those that were deposited on either glass or on polymer which had been pres-stamped. The exact cause of this remains unknown, though we hypothesize that the reason for this is the intrinsic stresses that are known to arise as a consequence of sputter deposition[72]. Once of the known causes for this intrinsic stress is the heating of the substrate and the deposited film. Typically, there will be some amount of mismatch between coefficients of thermal expansion such that when the substrate and film cool, there will be stresses arising at their interface. Such stresses can lead to dislocations and other defects which may impact the electrical properties of the deposited film. When depositing on a freestanding polymer film, the freestanding substrate is much more compliant than a rigid substrate and so the strain arising from thermal expansion mismatch are much more likely to be accommodated. Hence, this compliance would reduce the occurrence of stress-induced defects and result in improved electrical conductivity.

3.3 Device Integration

We used bilayer ITO/2DPP-2CNTVT films to create sputter-free transparent electrodes on the perovskite solar cells. We chose this polymer because we found it functioned reasonably well as an electron-transport layer (ETL) in control devices which used evaporated Ag as the analogous electrode. We found the most significant challenge in integrating these bilayer films into a completed device to be ensuring that good electrical contact was being made. This requirement was significantly complicated by the roughness of the perovskite surface. Because TCOs are highly stiff materials, with a low tensile fracture strain, achieving conformality poses a challenge that is not present when the TCO is sputtered directly onto the device stack. In order to facilitate good electrical contact, we spun a layer of 2DPP-2CNTVT onto the perovskite prior to transfer of the bilayer. This was done in order to help planarize the surface, provide a slightly more compliant interface, form a perovskite/polymer interface fully unaffected by sputtering, as well as to improve the wetting behaviour between the substrate and bilayer film arising from a

polymer/polymer interface.

When the films are transferred onto the device without further processing, we found the charge extraction to be essentially zero, as evidenced by the minuscule current densities extracted from the devices. However, the induced photovoltages in these devices were comparable to those of the evaporated Ag controls. This result suggested that the energetics at the interfaces were favorable for charge extraction, as there was sufficient quasi-Fermi level splitting to generate the photovoltage in the first place, but that ultimately most of that charge was not making it all the way to the electrode for extraction to the applied load.

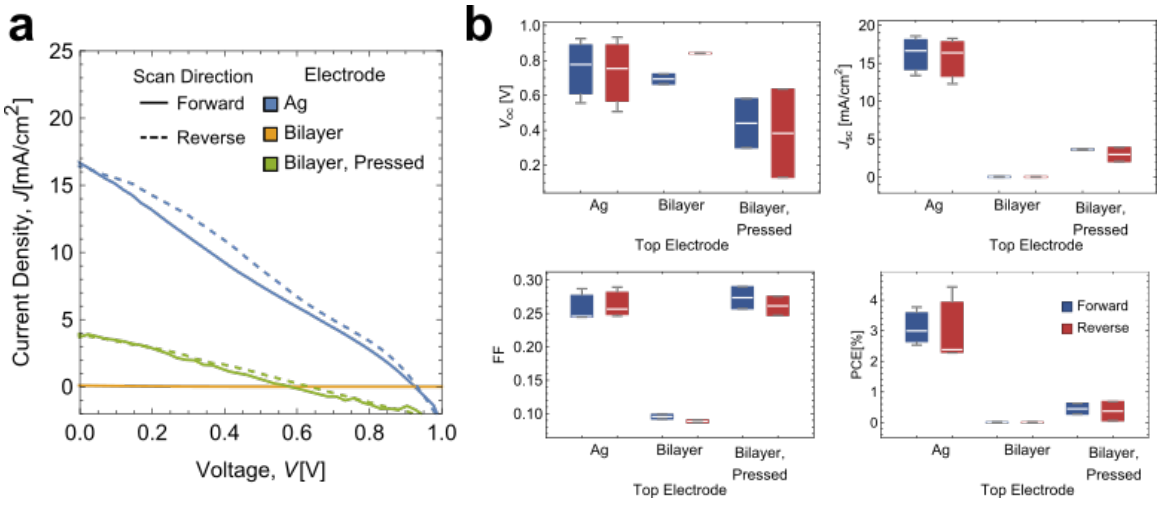

Figure 3.3. a) J-V curves of the champion perovskite devices for each condition, (blue) Ag top contact, (orange) bilayer top contact without further processing, (green) bilayer top contact after heat pressing at 150 °C and 2 MPa for 15 minutes. b) PV metrics for the devices in the various conditions.

To improve the electrical contact we subjected the cells to heat pressing. Akin to the lamination process that allows two perovskite films to recrystallize and fuse[73], we aimed to restructure the perovskite surface as well as reflow the polymer to promote inter-diffusion and further promote charge transport. The heat-pressing was done in air at a temperature of 150 °C and a pressure of 2 MPa for 15 minutes. The improvement in charge extraction was remarkable, as we observed an improvement of several orders of magnitude. Though the devices still underperformed compared to the controls with evaporated Ag electrodes, we believe that

with additional heat-press optimization, as well as strategies to reduce wrinkling of the ITO and smooth the perovskite surface, the performance of the transferred devices can be brought much more in line with the controls.

3.4 Experimental Methods

3.4.1 Preparation of the Freestanding Polymer Films

All film formations and drawing were performed on custom-built systems. All custom parts, such as roller drums, troughs, and substrate carriage were printed on a Form 3 SLA printer using Form Clear Resin. The troughs in particular were treated in air plasma for an extended period of time (>3 hr) to crosslink the print surface and minimize leeching of the monomers and oligomers into the water used for interfacial spreading. Furthermore, a hydrophobic silane treatment was applied to the trough surface to modify the water contact angle and planarize the water surface in order to avoid pooling of the polymer solution.

3.4.2 Mechanical Properties of Polymers

The mechanical properties of the P3ATs were cited from[1]. All other mechanical properties were measured using the psuedo-freestanding "film-on-water" tensile test, which has been described elsewhere[64]. All reported mechanical properties were from films prepared by interfacial spreading, and all gathered data can be found in Figure 2.9.

3.4.3 Polymer Film Characterization

3.4.4 Sample Preparation for Absorbance Spectroscopy and Sheet Resistance

Polymer Film Preparation: P3HpT was dissolved in chlorobenzene at a concentration of 20 mg/mL by stirring at 60 °C overnight. Each film was formed by interfacially spread by dropping 10 μL of solution where in a glass petri dish with a 6 cm diameter and filled with DI

water. The floating film was then mounted on frames (15 $\times$ 15 mm^2 freestanding dimensions) or transferred directly onto glass slides by stamping from the water surface.

TCO Film Sputtering: ITO was sputtered onto the freestanding polymer films, onto the pre-stamped films, or directly onto glass. The deposition was done in an Ar atmosphere at a pressure of 4 mTorr and an RF power of 60 W for a 2" diameter target. This resulted in a rate of ca. 0.54 Å/s and the deposition was performed for 30 minutes 50 seconds for a total thickness of ca. 100 nm.

3.4.5 Preparation of Perovskite Solar Cells

Substrate Preparation: Indium tin oxide (ITO) substrates were purchased pre-diced and pre-etched from Biotain Crystal Co. (TEC 8, 6-8 Ω/sq). They were cleaned by a series of sonication and washing steps as follows: sonicate in 2 vol% Hellmanex III in DI water for 15 min, rinse with DI water, sonicate in DI water for 15 min, rinse with DI water, sonicate in acetone (99.9% purity) for 15 min, rinse with DI water, sonicate in IPA (99.5% purity) for 15 min, then dry with filtered dry air. Immediately prior to further processing, the ITO substrates were UVO-treated for 15 min.

MeO-2PACz Hole Transport Layer: MeO-2PACz was dissolved in EtOH at a concentration of 0.6 mg/mL. This was spun onto the ITO substrates (5k RPM, 2k RPM/s, 30 s) and annealled at 100 °C for 60 s.

Perovskite Absorber: The selected perovskite composition has a nominal solution stoichiometry of $FA_{0.76}MA_{0.03}Cs_{0.21}Pb(I_{0.83}Br_{0.14}Cl_{0.03})_3$ dissolved in a 3:1 v/v mixture of DMF and DMSO at a 1.4 M concentration. The films were spin-coated (5000 RPM, 2000 RPM/s, 50 s) with a 200 μL drop of methylacetate 25 s into the spin. The resulting films were annealed at 100 °C for 30 min. All perovskite processing was conducted in a nitrogen-filled glovebox.

2DPP-2CNTVT Electron Transport Layer: 2DPP-2CNTVT was dissolved in anhydrous o-xylene at a concentration of 7 mg/mL and then filtered using a glass filter of 1 μm pore size. The solution was then spin-coated on the perovskite films (3000 RPM, 2000 RPM/s, 30 s) and

then annealed at 100 °C for 10 min.

Ag Top Electrode: A 100 nm layer of Ag was deposited by vacuum thermal evaporation for the control devices.

Bilayer Preperation: 2DPP-2CNTVT was dissolved in anhydrous chlorobenzene at a concentration of 15 mg/mL and interfacially spread in a rectangular trough (13.5 × 15.5 cm area) and drawn onto a single piece frame with multiple (36) freestanding "cells" (12 × 12 mm). ITO was sputtered directly onto the freestanding films. The deposition was done in an Ar atmosphere at a pressure of 4 mTorr and an RF power of 60 W for a 2" diameter target. This resulted in a rate of ca. 0.54 Å/s and the deposition was performed for 30 minutes 50 seconds for a total thickness of ca. 100 nm.

Top Electrode Transfer and Heat Pressing: The bilayer films were brought into a N_2 glovebox and transferred onto the perovskite half cells by gently lowering the films onto the cells using an alignment jig. The cells then underwent heat pressing in air at 150 °C and 2 MPa for 15 min.

JV Testing: After device fabrication was completed, the cells were allowed to age in nitrogen for 15 days, as this was observed to significantly improve the device fill factors by eliminating "double-diode" behaviour in the JV sweeps (Figure 2.14). Devices were tested in nitrogen environment using an ABET Mondel 11002 SunLite Solar Simulator, under AM 1.5G, at 100 mW/cm^2, with a scan speed of 0.1 V/s, and a fixed aperture of 0.07 cm^2. Prior to testing, the light intensity was calibrated using a standard silicon reference cell purchased from PV Measurements, Inc.

Chapter 3, in part is currently being prepared for submission for publication of the material. Guillermo L. Esparza, Deniz Cakan, Jaden Cramlet, Benjamin Wang, Jack Palmer, David P. Fenning, Darren J. Lipomi. The dissertation author was the primary investigator and author of this material.

Bibliography

[1] Choudhary, K.; Chen, A. X.; Pitch, G. M.; Runser, R.; Urbina, A.; Dunn, T. J.; Kodur, M.; Kleinschmidt, A. T.; Wang, B. G.; Bunch, J. A.; Fenning, D. P.; Ayzner, A. L.; Lipomi, D. J. *ACS Applied Materials and Interfaces* **2021**, *13*, 51436–51446.

[2] Alf, M. E.; Asatekin, A.; Barr, M. C.; Baxamusa, S. H.; Chelawat, H.; Ozaydin-lnce, G.; Petruczok, C. D.; Sreenivasan, R.; Tenhaeff, W. E.; Trujillo, N. J.; Vaddiraju, S.; Xu, J.; Gleason, K. K. *Advanced Materials* **2010**, *22*, 1993–2027.

[3] Esparza, G. L.; Lipomi, D. J. *ACS Materials Letters* **2021**, *3*, 988–995.

[4] Aydin, E.; Altinkaya, C.; Smirnov, Y.; Yaqin, M. A.; Zanoni, K. P.; Paliwal, A.; Firdaus, Y.; Allen, T. G.; Anthopoulos, T. D.; Bolink, H. J.; Morales-Masis, M.; De Wolf, S. *Matter* **2021**, *4*, 3549–3584.

[5] Gudmundsson, J. T.; Lundin, D. *High Power Impulse Magnetron Sputtering: Fundamentals, Technologies, Challenges and Applications*; 2019; pp 1–48.

[6] Al-Husseini, A. M.; Lahlouh, B. *Bulletin of Materials Science* **2019**, *42*, 152.

[7] Jošt, M.; Köhnen, E.; Morales-Vilches, A. B.; Lipovšek, B.; Jäger, K.; Macco, B.; Al-Ashouri, A.; Krč, J.; Korte, L.; Rech, B.; Schlatmann, R.; Topič, M.; Stannowski, B.; Albrecht, S. *Energy and Environmental Science* **2018**, *11*, 3511–3523.

[8] Esparza, G. L.; Kodur, M.; Chen, A. X.; Wang, B.; Bunch, J. A.; Cramlet, J.; Runser, R.; Fenning, D. P.; Lipomi, D. J. *Advanced Materials* **2023**, *2207798*, 1–7.

[9] Noh, J.; Jeong, S.; Lee, J. Y. *Nature Communications* **2016**, *7*.

[10] Meng, X. *Journal of Materials Chemistry A* **2017**, *5*, 18326–18378.

[11] Kim, J. B.; Kim, P.; Pégard, N. C.; Oh, S. J.; Kagan, C. R.; Fleischer, J. W.; Stone, H. A.; Loo, Y. L. *Nature Photonics* **2012**, *6*, 327–332.

[12] He, J.; Wan, Y.; Gao, P.; Tang, J.; Ye, J. *Advanced Functional Materials* **2018**, *28*, 1802192.

[13] Hou, Y. et al. *Science* **2020**, *367*, 1135–1140.

[14] Buskens, P.; Burghoorn, M.; Mourad, M. C. D.; Vroon, Z. *Langmuir* **2016**, *32*, 6781–6793.

[15] Brown, P. S.; Bhushan, B. *Scientific Reports* **2015**, *5*, 1–9.

[16] Tanaka, M.; Sackmann, E. *Nature* **2005**, *437*, 656–663.

[17] Bronner, I. F.; Quail, M. A. *Current Protocols in Human Genetics* **2019**, *102*, 86.

[18] Atwater, H. A.; Polman, A. *Nature Materials* **2010**, *9*, 205–213.

[19] Manzoor, S.; Filipič, M.; Onno, A.; Topič, M.; Holman, Z. C. *Journal of Applied Physics* **2020**, *127*, 063104.

[20] Minko, S. *Polymer Surfaces and Interfaces: Characterization, Modification and Applications*; Springer Berlin Heidelberg, 2008; pp 215–234.

[21] Higaki, Y.; Kobayashi, M.; Hirai, T.; Takahara, A. *Polymer Journal* **2018**, *50*, 101–108.

[22] Alkekhia, D.; Hammond, P. T.; Shukla, A. *Annual Review of Biomedical Engineering* **2020**, *22*, 1–24.

[23] Patterson, R.; Kandelbauer, A.; Müller, U.; Lammer, H. *Handbook of Thermoset Plastics*; 2014; pp 697–737.

[24] Clark, S. L.; Hammond, P. T. *Advanced Materials* **1998**, *10*, 1515–1519.

[25] Isarov, S. A.; Pokorski, J. K. *ACS Macro Letters* **2015**, *4*, 969–973.

[26] Yoon, J. A.; Kowalewski, T.; Matyjaszewski, K. *Macromolecules* **2011**, *44*, 2261–2268.

[27] Bergsman, D. S.; Closser, R. G.; Tassone, C. J.; Clemens, B. M.; Nordlund, D.; Bent, S. F. *Chemistry of Materials* **2017**, *29*, 1192–1203.

[28] Mulhearn, W. D.; Stafford, C. M. *ACS Applied Polymer Materials* **2021**, *3*, 116–121.

[29] Allison, L.; Hoxie, S.; Andrew, T. L. *Chemical Communications* **2017**, *53*, 7182–7193.

[30] Bilger, D.; Homayounfar, S. Z.; Andrew, T. L. *Journal of Materials Chemistry C* **2019**, *7*, 7159–7174.

[31] Root, S. E.; Savagatrup, S.; Printz, A. D.; Rodriquez, D.; Lipomi, D. J. *Chemical Reviews* **2017**, *117*, 6467–6499.

[32] O'Connor, T. F.; Zaretski, A. V.; Shiravi, B. A.; Savagatrup, S.; Printz, A. D.; Diaz, M. I.; Lipomi, D. J. *Energy and Environmental Science* **2014**, *7*, 370–378.

[33] Meitl, M. A.; Zhu, Z. T.; Kumar, V.; Lee, K. J.; Feng, X.; Huang, Y. Y.; Adesida, I.; Nuzzo, R. G.; Rogers, J. A. *Nature Materials* **2006**, *5*, 33–38.

[34] Harnois, M.; Himdi, M.; Yong, W. Y.; Rahim, S. K. A.; Tekkouk, K.; Cheval, N. *Scientific Reports* **2020**, *10*, 1–8.

[35] Savagatrup, S.; Makaram, A. S.; Burke, D. J.; Lipomi, D. J. *Advanced Functional Materials* **2014**, *24*, 1169–1181.

[36] Li, J.; Zhao, Y.; Tan, H. S.; Guo, Y.; Di, C. A.; Yu, G.; Liu, Y.; Lin, M.; Lim, S. H.; Zhou, Y.; Su, H.; Ong, B. S. *Scientific Reports* **2012**, *2*, 1–9.

[37] O'Connor, B.; Chan, E. P.; Chan, C.; Conrad, B. R.; Richter, L. J.; Kline, R. J.; Heeney, M.; McCulloch, I.; Soles, C. L.; DeLongchamp, D. M. *ACS Nano* **2010**, *4*, 7538–7544.

[38] Runser, R.; Root, S. E.; Ober, D. E.; Choudhary, K.; Chen, A. X.; Dhong, C.; Urbina, A. D.; Lipomi, D. J. *Chemistry of Materials* **2019**, *31*, 9078–9086.

[39] Owens, D. K.; Wendt, R. C. *Journal of Applied Polymer Science* **1969**, *13*, 1741–1747.

[40] Wu, S. *Journal of Polymer Science Part C: Polymer Symposia* **2007**, *34*, 19–30.

[41] Girifalco, L. A.; Good, R. J. *Journal of Physical Chemistry* **1957**, *61*, 904–909.

[42] Gupta, M.; Gleason, K. K. *Langmuir* **2006**, *22*, 10047–10052.

[43] Colberts, F. J.; Wienk, M. M.; Heuvel, R.; Li, W.; Le Corre, V. M.; Koster, L. J. A.; Janssen, R. A. *Advanced Energy Materials* **2018**, *8*, 1802197.

[44] Ellison, C. J.; Torkelson, J. M. *Nature Materials* **2003**, *2*, 695–700.

[45] Galuska, L. A.; Muckley, E. S.; Cao, Z.; Ehlenberg, D. F.; Qian, Z.; Zhang, S.; Rondeau-Gagné, S.; Phan, M. D.; Ankner, J. F.; Ivanov, I. N.; Gu, X. *Nature Communications* **2021**, *12*, 1–11.

[46] Priestley, R. D.; Ellison, C. J.; Broadbelt, L. J.; Torkelson, J. M. *Science* **2005**, *309*, 456–459.

[47] Alcoutlabi, M.; McKenna, G. B. *Journal of Physics Condensed Matter* **2005**, *17*, R461.

[48] Pushparaj, V. L.; Shaijumon, M. M.; Kumar, A.; Murugesan, S.; Ci, L.; Vajtai, R.; Lin-

hardt, R. J.; Nalamasu, O.; Ajayan, P. M. **2007**, *104*.

[49] Markutsya, S.; Jiang, C.; Pikus, Y.; Tsukruk, V. V. *Advanced Functional Materials* **2005**, *15*, 771–780.

[50] Taccola, S.; Greco, F.; Zucca, A.; Innocenti, C.; De Julián Fernández, C.; Campo, G.; Sangregorio, C.; Mazzolai, B.; Mattoli, V. *ACS Applied Materials and Interfaces* **2013**, *5*, 6324–6332.

[51] Ulbricht, M. *Polymer* **2006**, *47*, 2217–2262.

[52] Fujie, T.; Matsutani, N.; Kinoshita, M.; Okamura, Y.; Saito, A.; Takeoka, S. *Advanced Functional Materials* **2009**, *19*, 2560–2568.

[53] Okamura, Y.; Kabata, K.; Kinoshita, M.; Saitoh, D.; Takeoka, S. *Advanced Materials* **2009**, *21*, 4388–4392.

[54] Cheng, W.; Campolongo, M. J.; Tan, S. J.; Luo, D. *Nano Today* **2009**, *4*, 482–493.

[55] Stadermann, M.; Baxamusa, S. H.; Aracne-Ruddle, C.; Chea, M.; Li, S.; Youngblood, K.; Suratwala, T. *Journal of Visualized Experiments* **2015**, *2015*, e52832.

[56] Kang, S.; Pyo, J. B.; Kim, T. S. *Langmuir* **2018**, *34*, 5831–5836.

[57] Greco, F.; Zucca, A.; Taccola, S.; Menciassi, A.; Fujie, T.; Haniuda, H.; Takeoka, S.; Dario, P.; Mattoli, V. *Soft Matter* **2011**, *7*, 10642–10650.

[58] Pandey, M.; Pandey, S. S.; Nagamatsu, S.; Hayase, S.; Takashima, W. *Thin Solid Films* **2016**, *619*, 125–130.

[59] Kim, Y. J.; Jung, H. T.; Ahn, C. W.; Jeon, H. J. *Advanced Materials Interfaces* **2017**, *4*, 1700342.

[60] Bard, A. J.; Faulkner, L. R. *Russian Journal of Electrochemistry 2002 38:12* **2002**, *38*, 1364–1365.

[61] Kodur, M.; Dorfman, Z.; Kerner, R. A.; Skaggs, J. H.; Kim, T.; Dunfield, S. P.; Palmstrom, A.; Berry, J. J.; Fenning, D. P. *ACS Energy Letters* **2022**, *7*, 683–689.

[62] Swartwout, R.; Hoerantner, M. T.; Bulović, V. *Energy and Environmental Materials* **2019**, *2*, 119–145.

[63] Zhou, Y.; Najar, A.; Zhang, J.; Feng, J.; Cao, Y.; Li, Z.; Zhu, X.; Yang, D.; Liu, S. F. *ACS Applied Materials & Interfaces* **2022**, *14*, 28729–28737.

[64] Kim, J. H.; Nizami, A.; Hwangbo, Y.; Jang, B.; Lee, H. J.; Woo, C. S.; Hyun, S.; Kim, T. S. *Nature Communications* **2013**, *4*, 1–6.

[65] Connelly, N. G.; Geiger, W. E. *Chemical Reviews* **1996**, *96*, 877–910.

[66] Belo, G. S.; da Silva, B. J.; de Vasconcelos, E. A.; de Azevedo, W. M.; da Silva, E. F. *Applied Surface Science* **2008**, *255*, 755–757.

[67] Werner, J.; Geissbühler, J.; Dabirian, A.; Nicolay, S.; Morales-Masis, M.; Wolf, S. D.; Niesen, B.; Ballif, C. *ACS Applied Materials and Interfaces* **2016**, *8*, 17260–17267.

[68] Raiford, J. A.; Belisle, R. A.; Bush, K. A.; Prasanna, R.; Palmstrom, A. F.; McGehee, M. D.; Bent, S. F. *Sustainable Energy and Fuels* **2019**, *3*, 1517–1525.

[69] Aydin, E. et al. *Energy and Environmental Science* **2021**, *14*, 4377–4390.

[70] Zhao, W.; Duan, Y. *Advanced Photonics Research* **2021**, *2*, 2100011.

[71] Hoffmann, L.; Brinkmann, K. O.; Malerczyk, J.; Rogalla, D.; Becker, T.; Theirich, D.; Shutsko, I.; Görrn, P.; Riedl, T. *ACS Applied Materials and Interfaces* **2018**, *10*, 6006–6013.

[72] Koenig, T. R.; Rao, Z.; Chason, E.; Tucker, G. J.; Thompson, G. B. *Surface and Coatings Technology* **2021**, *412*, 126973.

[73] Dunfield, S. P.; Moore, D. T.; Klein, T. R.; Fabian, D. M.; Christians, J. A.; Dixon, A. G.; Dou, B.; Ardo, S.; Beard, M. C.; Shaheen, S. E.; Berry, J. J.; Van Hest, M. F. *ACS Energy Letters* **2018**, *3*, 1192–1197.